Title

Transcriptional Repression of *reaper* by Stand Still Safeguards Female Germline Development in *Drosophila*

Authors

Masaya Matsui[1], Shinichi Kawaguchi[1], and Toshie Kai[1]*

*Corresponding author

E-mail: kai.toshie.fbs@osaka-u.ac.jp (KT)

Affiliations

[1] Graduate School of Frontier Biosciences, The University of Osaka, Osaka 565-0871, Japan

Abstract

Apoptosis plays a central role in shaping tissues and preserving cellular integrity across developmental stages. In the germline, its precise regulation is critical to ensure both the elimination of aberrant cells and the maintenance of reproductive capacity. However, the molecular mechanisms that control apoptotic susceptibility in germline cells remain poorly defined. Here, we identify *stand still* (*stil*) as a female germline-specific regulator of apoptosis in *Drosophila*. Loss of *stil* leads to near-complete depletion of germline cells at the time of eclosion, associated with upregulation of the pro-apoptotic gene *reaper* (*rpr*) and activation of caspase-dependent cell death. Reporter assays in S2 cells show that Stil directly represses *rpr* transcription through its N-terminal BED-type zinc finger domain. Despite the absence of *stil*, undifferentiated germline cells remain resistant to apoptosis. Analysis of publicly available chromatin data reveals that the *rpr* locus in these cells resides in a closed, H3K9me3-enriched chromatin state, suggesting a Stil-independent mode of transcriptional silencing. Together, our findings uncover a dual mechanism that protects the female germline from *rpr*-dependent apoptosis: active repression by Stil in differentiating cells and chromatin-mediated silencing in undifferentiated cells. This work provides new insights into the transcriptional and chromatin-based mechanisms that maintain germline cell identity and survival.

Introduction

Apoptosis, a form of programmed cell death (PCD), is a highly regulated biological process essential for animal development and tissue homeostasis. *Drosophila* is an excellent model organism for studying apoptotic cell death, due to its powerful genetic and molecular tools. In Drosophila, apoptosis is often initiated by the expression of IAP (inhibitor of apoptosis) antagonists, including members of the RHG gene family: *reaper* (*rpr*), *hid* (*head involution defective*), *grim*, and *sickle* (*skl*) (Abbott & Lengyel, 1991; P. Chen et al., 1996; Christich et al., 2002; White et al., 1994). Among these, the pro-apoptotic gene *rpr* plays a central role in PCD and stress-induced apoptosis (Yan et al., 2004). The *Drosophila* IAP protein DIAP1 is degraded via auto-ubiquitination, triggered by the physical interaction of Rpr through its conserved IAP-binding motif (IBM), leading to caspase activation and apoptotic cell death (Holley et al., 2002; Sandu et al., 2010). *rpr* expression is regulated by transcription factors and histone modifications, such as H3K27 and H3K9 trimethylation, in response to developmental and environmental signals (Beira et al., 2014; Brodsky et al., 2000; Jiang et al., 2000; Lohmann et al., 2002; Zhang et al., 2008).

For reproductive success, apoptosis is meticulously regulated to control cell numbers and maintain germline cell quality (Almeida et al., 2013; Chaudhry et al., 2021; Huang et al., 2023; Knudson et al., 1995). *Drosophila* adult female has a pair of ovaries, each containing 16–20 ovarioles. At the apical end of each ovariole lies the germarium, which houses germline stem cells (GSCs) that divide asymmetrically to produce a self-renewing GSC and a cystoblast. Cystoblast undergoes four mitotic divisions to form a 16-cell cyst

63 interconnected by ring canals. Of these 16 cells, one differentiates into the
64 oocyte and enters meiosis, while the remaining 15 become nurse cells that
65 support the oocyte by transporting proteins and RNAs. Encapsulated by
66 somatic follicle cells, the cysts develop into egg chambers that progress
67 through 14 stages, culminating in mature, fertilizable eggs (Gleason et al.,
68 2018; Spradling et al., 2001).

69 To safeguard the fidelity of this process, apoptosis operates at two
70 key checkpoints —within the germarium and during mid-oogenesis —ensuring
71 that only healthy cells contribute to egg development. In the germarium, the
72 first checkpoint triggers apoptotic cell death in response to DNA damage,
73 mediated by p53-induced *hid* expression rather than *rpr* (Hou et al., 2008;
74 Park et al., 2019). At the second checkpoint during mid-oogenesis, germline
75 cells undergo caspase-regulated apoptotic and autophagic cell death in
76 nutrient deprived condition, even though RHG genes are dispensable.
77 (Baonza et al., 2022; Jeanne S. Peterson et al., 2007; T L Pritchett & McCall,
78 2012; Xing et al., 2015). Although apoptotic cell death is intricately regulated
79 in response to various stimuli during oogenesis, the involvement of *rpr* in
80 germline apoptosis remains largely unknown. Previous studies have identified
81 *stand still* (*stil*) as a critical regulator of *Drosophila* germline cell survival
82 (Schüpbach & Wieschaus, 1989). Genetic interactions with female germline-
83 specific genes, such as *ovo* and *ovarian tumor* (*otu*), along with the female
84 germline-specific requirement of *stil*, suggested its involvement in sex
85 determination (G & D., 1997; Sahut-Barnola & Pauli, 1999). However, how Stil
86 controls germline cell fate remains unknown. In this study, we identify *stil* as a
87 repressor of *rpr* in female germline cells. Loss of *stil* function led to apoptosis-

88 mediated depletion of ovarian germline cells, associated with *rpr* upregulation.
89 Stil was enriched at the *rpr* locus and its upstream transcriptional control
90 region, suggesting a direct role in *rpr* regulation. Reporter assays in
91 *Drosophila* S2 cells revealed that Stil represses *rpr* transcription via its N-
92 terminal BED-type zinc finger domain, indicating its role as a repressive
93 transcription factor. In addition, we found that undifferentiated germline stem
94 cell (GSC)-like cells, in which the *rpr* locus exhibits a closed chromatin
95 structure, were resistant to apoptosis caused by *stil* loss. Our findings reveal a
96 molecular mechanism by which Stil and chromatin accessibility repress *rpr*,
97 providing novel insights into the regulation of germline cell fate.
98

99 **Results**

100 **Loss of *stand still* (*stil*) leads to female germline cell loss**

101 Previous studies have demonstrated the necessity of *standstill* (*stil*)
102 function in female germline cells; however, its molecular role remains elusive
103 (G & D., 1997; PK et al., 1996). To address this, we analyzed a loss of
104 function allele, $stil^{EY16156}$, which harbors a P-element insertion near the 3'end
105 of the second exon of *stil* gene, potentially disrupting the splicing of *stil*
106 transcripts (Fig 1A) (Bellen et al., 2004, 2011). RT-PCR revealed that *stil*
107 transcripts were undetectable in homozygous $stil^{EY16156}$ ovaries and in
108 $stil^{EY16156}$ testes, indicating a complete loss of *stil* expression in both gonads
109 (Fig. 1B).

110 Similar to the previously reported loss-of-function allele $stil^{3}$, which exhibited
111 the most severe phenotype (Fig. 1A; Fig. S1A, B) (PK et al., 1996), ovaries of
112 both $stil^{EY16156}$ homozygous and $stil^{EY16156}/Df(2R)vg\text{-}C$ trans-heterozygote, in
113 which the deficiency uncovers the entire *stil* locus, were severely reduced in
114 size and completely lacked germline cells (Fig. 1C, D). Likewise, $stil^{3}/stil^{EY16156}$
115 trans-heterozygote females exhibited more severe germline cell loss than
116 $stil^{3}/Df(2R)vg\text{-}C$ (Fig. S1A, B). However, male germline cell in $stil^{EY16156}$ testes
117 progressed to differentiate into mature sperms (Fig.S1A). Notably, fertility
118 assayed by egg production and hatching rate, was comparable between
119 $stil^{EY16156}$ and $stil^{EY16156}/CyO$ males (Fig. S1B), indicating that *stil* is specifically
120 required for female germline cells. The loss of germline cell in $stil^{EY16156}$
121 ovaries was fully rescued by overexpression of the *UASp-6×Myc-Stil*
122 transgene, driven by the germline-specific *NGT40; Nos-Gal4-VP16* driver
123 (Fig. 1C, D) (Grieder et al., 2000). Mutant females expressing 6×Myc-Stil,

124 germline cells were differentiated and developed into mature eggs that
125 hatched comparably to those of heterozygous control (Fig. 1E). Collectively,
126 these results confirm the pivotal role of *stil* in maintaining female germline
127 cells and ensuring proper oogenesis.
128
129 **_stil_-deficient germline cells undergo apoptotic cell death**
130 To investigate the cause of female germline cell loss, we knocked down *stil*
131 function by expressing short hairpin RNA targeting the 4th exon of the *stil*
132 transcript (GL01230) using a germline driver (Fig. 1A). Germline-specific
133 knockdown (*stil*-GLKD) reduced *stil* expression in ovaries by approximately
134 90% compared to control (Fig. 2A). *stil*-GLKD females contained significantly
135 smaller ovaries and did not lay any eggs, resembling to *stil* loss-of-function
136 mutant females (Fig. 2B and Fig. S2A). Unlike the complete germline loss
137 observed in *stil* mutants, however, most ovarioles in *stil*-GLKD retained
138 germline cells, indicating a milder phenotype (Fig. 2C). Notably, the number of
139 ovarioles containing at least two egg chambers was remarkably fewer (27.4%
140 versus 100% in the control), suggesting that oogenesis was perturbed before
141 mid-oogenesis (Fig. 2B, D). While *stil*-GLKD exhibited severe defects similar
142 to its loss-of function alleles, its somatic knockdown using a tj-Gal4 driver (*stil*-
143 STKD) did not affect egg production and the hatching rate at all (Fig. S2A).
144 These observations suggest that *stil* functions in germline cells both for the
145 survival of female germline cells and egg development.
146 Previous studies have suggested that stil may play a role in sex
147 determination, particularly through its genetic interaction with *ovo* and the key
148 sex determination regulator *otu*, which represses the male identity factor

149 Tdrd5l (G & D., 1997; Primus et al., 2019; Sahut-Barnola & Pauli, 1999) . To
150 investigate whether *stil* is involved in sex determination, we examined the
151 transcripts of *sxl*, a master regulator of sex determination of germline cells in
152 *stil* mutant ovaries (Hashiyama et al., 2011). *sxl* pre-mRNA undergoes
153 alternative splicing to generate sex-specific isoforms, producing a functional
154 Sxl protein essential for female development, or a truncated non-functional
155 male-specific isoform (Bell et al., 1991) (Moschall et al., 2019). RT-PCR
156 revealed an enrichment of the female-specific *sxl* isoform in both control and
157 *stil*-GLKD ovaries (Fig. S2B). In addition, male-specific *sxl* transcripts,
158 detected in both control and *stil*-GLKD testes, were absent in *stil*-GLKD
159 ovaries, indicating that *sxl* splicing patterns remain unaffected by *stil*
160 depletion. These results suggest that *stil* functions independently of sex
161 identity determination in germline cells.
162 Damaged or abnormal cells are typically removed through regulated cell
163 death mechanisms, including apoptosis, autophagy, and necrosis (Fuchs &
164 Steller, 2011, 2015). In *Drosophila* ovaries, such cell death occurs at two
165 distinct developmental checkpoints during oogenesis: in the germarium and
166 during mid-oogenesis, in response to either developmental cues or
167 environmental stressors (McCall, 2004; Tracy L. Pritchett et al., 2009). To
168 determine whether germline cell loss in *stil*-deficient ovaries was due to
169 apoptosis, we performed a TUNEL (Terminal deoxynucleotidyl Transferase
170 Biotin dUTP Nick End Labeling) assay, which detects DNA fragmentation
171 indicative of apoptotic cell death. In region 2A and 2B of the germarium, the
172 first developmental checkpoint in oogenesis (Drummond-Barbosa &
173 Spradling, 2001), the number of TUNEL-positive cells significantly increased

174 in *stil*-GLKD ovaries compared to controls (Fig. 2E, F). These results suggest
175 that *stil*-GLKD germline cells undergoes apoptotic cell death.
176 To further confirm the involvement of *stil* in apoptosis, we overexpressed
177 inhibitor of apoptosis proteins (IAPs) in *stil* mutant germline cells. Both the
178 *Drosophila* protein DIAP1 (Death-associated inhibitor of apoptosis 1) and the
179 baculovirus-derived P35 are well-characterized inhibitors that can effectively
180 suppress apoptosis in *Drosophila*. DIAP1 inhibits the activity of initiator
181 caspase, Dronc (Death regulator Nedd2-like caspase) which activates effector
182 caspase, while P35 directly inhibits effector caspase (Baum et al., 2007; J.S
183 Peterson et al., 2003; Werz et al., 2005). Germline-specific overexpression of
184 P35 fully rescued the germline cell loss observed in $stil^{EY16156}$ mutants (Fig.
185 2G, H). However, germline development remained arrested, and egg
186 chambers degenerated at the mid-oogenesis (Fig. S3). Likewise, DIAP1
187 overexpression partially restored germline cells (~50% of ovarioles retained
188 germline cells), but did not fully rescue oogenesis defects (Fig. 2G, H).
189 Altogether, these findings indicate that the loss of *stil* function not only triggers
190 apoptosis that can be suppressed by apoptosis inhibitors but also causes
191 defects in oogenesis progression that are not rescued by blocking cell death.
192

193 **Stil regulates proapoptotic genes to suppress apoptosis in female**
194 **germline cells**

195 Stil protein harbors a characteristic DNA-binding domain, BED-type zinc
196 finger, containing highly conserved aromatic residues followed by a shared
197 pattern of cysteines and histidines (Fig. S4A) (Aravind, 2000). Given that
198 many of the known BED-type zinc fingers including the founder members,

199 BEAF and DREF, function as transcription factors or chromatin regulators
200 (McKowen et al., 2022; Sokolova et al., 2023; Tue et al., 2017), Stil may play
201 a role in transcriptional regulation. To examine this possibility, we analyzed
202 the transcriptional profiles of ovarian RNA of *stil* mutant and control. We took
203 advantage of the ectopic expression of P35 to overcome cell death defect of
204 germline cells due to the loss of in *stil* function. The RNA-seq analysis
205 identified 3,569 (30.7%) differentially expressed genes (DEGs) (log2FC>|1|
206 and p-adj<0.01) out of 11,608 annotated genes (PRJDB20709;
207 Supplementary Table 1). Among these, 2,044 genes were up-regulated
208 (17.6 %, red dots) and 1,525 genes were down-regulated (13.1 %, blue dots)
209 in *stil* mutant ovaries (Fig. S4B). Consistent with the observation of
210 developmental arrest and egg chambers degeneration at the mid-stage of
211 oogenesis (Fig. S3), genes known to be highly expressed in late-stage
212 oogenesis, such as proteins composing the chorion, were significantly
213 downregulated in *stil* mutant ovaries (Fig. 3A). Of those upregulated, notably,
214 the proapoptotic gene *rpr* (*reaper*) ranked among the top 10 upregulated
215 DEGs (Fig. 3A). Given the apoptotic phenotype of *stil* mutant germline cells,
216 67 apoptosis-related genes out of 224 annotated in the dataset (GO:0006915)
217 were identified as DEGs (Fig. 3B). Among the top 10 genes list of apoptosis-
218 related DEGs, proapoptotic genes, *rpr* and *hid* (*head involution defective*),
219 were significantly upregulated, while the hedgehog signaling genes expressed
220 in later oogenesis such as *ptc*, *duox*, and *rdx* were significantly downregulated
221 (Fig. 3C). *rpr* and *hid* are the key members of IAP antagonists, known for their
222 central role in initiating apoptosis (Abbott & Lengyel, 1991; White et al., 1994).
223 Their activation through various signaling pathways leads to the ubiquitin-

224 mediated degradation and translational inhibition of DIAP1, which
225 subsequently results in the activation of Caspase proteins (Freel et al., 2008;
226 Holley et al., 2002). Further validation by RT-qPCR demonstrated that *rpr*
227 expression increased approximately 700-fold, while *hid* expression increased
228 15-fold in the rescued *stil* mutant ovaries by P35 expression (Fig. 3D). To
229 exclude a possibility that egg chamber degeneration in germline-rescued *stil*
230 mutants affects proapoptotic gene expression, we isolated RNAs from early-
231 stage ovaries (up to stage 5-6 of oogenesis) by manual removal of later
232 stages and re-examined their expression levels. *rpr* expression remained
233 elevated in RNAs prepared from early-stage ovaries, while *hid* expression did
234 not (Fig. S4B). Furthermore, RT-qPCR analysis using *stil*-GLKD ovaries
235 driven by three different germline drivers, *NGT40*; *NosGal4-VP16*, *Bam-Gal4*,
236 and *mat*α *-Tub-Gal4*, consistently exhibited significant upregulation of *rpr* but
237 not *hid* across all conditions (Fig. S5A). Conversely, *rpr* was not prominently
238 upregulated in *stil*-GLKD testes with *NGT40*; *NosGal4-VP16* or *Bam-Gal4*,
239 consistent with the phenotypic observations in *stil* mutant testes (Fig. S5C).
240 These results suggest that *rpr* is robustly upregulated in the absence of *stil*
241 function in female germline cells.
242 To determine whether proapoptotic genes upregulation directly contributes to
243 apoptosis of *stil* mutant female germline cells, we generated double mutants
244 of *stil* and the proapoptotic gene, *rpr*. Strikingly, the germline cell death and
245 differentiation defects observed in *stil* mutant ovaries were fully rescued in the
246 double mutant ovaries (Fig. 3E, F). Germline development proceeded,
247 resulting in the formation of mature eggs and partial restoration of fertility;
248 mutant females laid a few eggs and approximately 40 % of those hatched

249 (Fig. 3G, H). In contrast, *stil-hid* double mutants showed a slight increase in
250 germline cell survival, but no developing egg chambers were observed (Fig.
251 S5D, E), indicating that *hid* does not play a central role in apoptosis caused by
252 the loss of *stil* function. These findings highlight that *rpr* regulation by *stil* is
253 critical for suppressing apoptosis in female germline cells, establishing *rpr* as
254 a key downstream effector in this pathway.
255

256 **Stil represses *rpr* expression by targeting the regulatory regions via its**
257 **BED-type zinc finger**

258 The transcription of *rpr* is governed by a complex network of
259 developmental, environmental, and stress-related signals, each employing
260 distinct regulatory mechanisms. These signals modulate transcription factors
261 such as p53, Dfd, the EcR/USP complex, AP-1, Shn, leading to either the
262 activation or suppression of apoptosis (Beira et al., 2014; Brodsky et al., 2000;
263 Jiang et al., 2000; Lohmann et al., 2002). These transcription factors interact
264 with upstream enhancer and promoter regions of the *rpr* locus (*rpr*-
265 transcriptional control region) to either activate or suppress its transcription,
266 ensuring precise spatial and temporal control of apoptosis (Fuchs & Steller,
267 2011). To examine whether Stil also directly interacts with *rpr*-transcriptional
268 control region, we performed DNA adenine methyltransferase identification
269 (DamID)-seq analysis (Aughey et al., 2019). A fusion of Stil with *E. coli* DNA
270 adenine methyltransferase (Dam-Stil) or Dam alone as a control were
271 expressed specifically in germline cells (Díaz-Torres et al., 2021; Southall et
272 al., 2013). Genomic DNA from ovaries was digested with DpnI and subjected
273 to NGS to detect GATC sites methylated by Dam-Stil near Stil-bound regions

274 (PRJDB20722). Genome-wide DamID-seq analysis revealed that ~80% of
275 Stil-enriched peaks were located in promoter regions, supporting a role for Stil
276 in transcriptional regulation (Fig. 4A). At higher resolution, prominent peaks
277 were observed at the *rpr* locus and its upstream region (5–6 kb), suggesting
278 direct binding of Stil to the *rpr* regulatory element (Fig. 4B).Next, we examined
279 the role of Stil's BED-type zinc finger in *rpr* repression by generating four Stil
280 variants: Stil-FL (full-length), Stil-NT (N-terminal domain containing the BED-
281 type zinc finger and nuclear localization signal), Stil-CT (C-terminal domain
282 lacking these two motifs), and Stil-AAYA (full-length Stil with a mutated BED-
283 type zinc finger substituting four residues including two critical cysteines) (Fig.
284 4C). In nurse cells, despite lacking the predicted nuclear localization signal,
285 Stil-CT localized to the nucleus and overlapped with chromosomes, as did
286 Stil-FL and Stil-AAYA, whereas Stil-NT showed diffuse nuclear distribution
287 without being enriched onto chromosomes (Fig. S6A). Collectively, these data
288 suggest that Stil's nuclear and chromatin localization are mediated by the C-
289 terminal domain, independently of the zinc finger motif. To assess the
290 functional significance of these domains *in vivo*, we expressed the variants in
291 *stil*^{EY16156} germline cells. Stil-FL fully rescued the defects of both germline cell
292 survival and development, leading to the production of mature eggs (Fig. 4D,
293 E, F). Remarkably, Stil-NT partially rescued germline defects despite its
294 diffuse nuclear localization, while neither Stil-CT nor Stil-AAYA, both lacking
295 functional BED-type zinc fingers, restored germline cell survival or
296 differentiation. These findings suggest that the BED-type zinc finger is
297 essential for Stil function in germline cells possibly as a transcription regulator,
298 while the C-terminal domain mediates nuclear and chromatin localization.

299 To validate whether the BED-type zinc finger functions in *rpr* repression
300 through interaction with the *rpr* transcriptional control region, we performed a
301 reporter assay using *Drosophila* S2 cells. We constructed a *rpr*-GFP reporter
302 containing the 5-kb upstream region of *rpr*, where DamID-seq signals were
303 detected, fused to GFP (Fig. 4G) and transfected with Still variants. Stil
304 variants exhibited localization patterns in S2 cells similar to those in nurse
305 cells (Fig. S6B), supporting their suitability for functional analysis in S2 cells.
306 Consistent with the *in vivo* rescue experiment (Fig.4 D-F), co-expression of
307 Stil-FL with the *rpr*-GFP reporter significantly repressed GFP expression. Stil-
308 NT containing the BED-type zinc finger also reduced GFP expression, albeit
309 partially. In contrast, Stil-CT and Stil-AAYA failed to exhibit any detectable
310 repressive effects (Fig. 4H). To confirm the specificity of this Stil-mediated
311 repression, we utilized a *tubP*-GFP reporter containing the *αTub84B* gene
312 promoter fused to GFP (Fig. S6C)(Brennecke et al., 2003). Co-expression of
313 Stil-FL with the *tubP*-GFP reporter led to a modest reduction in GFP
314 expression, while other variants showed no discernible effect (Fig. S6D). This
315 effect was markedly weaker than the repression observed with the *rpr*-GFP
316 reporter, suggesting that Stil preferentially targets the *rpr* upstream region.
317 These results demonstrate that Stil interacts with the *rpr* transcriptional control
318 region via its BED-type zinc finger, which is critical for transcriptional
319 repression, while the chromatin association through the C-terminal region is
320 required for full repressive activity in germline cells.
321

322 **Undifferentiated Germline Cells Exhibit Resistance to Apoptosis in *stil***
323 **loss**

324 Loss of *stil* function resulted in severe depletion of germline cells by the 3rd
325 instar larval stage (120 hours after egg laying, AEL), leaving only a few
326 surviving germline cells in *stil* mutant (Fig. 5A, B). Notably, these surviving
327 germline cells were predominantly found near the terminal filaments and
328 future cap cells, the niche that supports germline stem cell (GSC) (Fig.
329 5A)(Spradling et al., 2001). This observation suggested that GSCs within the
330 niche may be resistant to cell death caused by *stil* loss. To test whether GSCs
331 are inherently resistant to cell death caused by *stil* deficiency, we induced
332 GSC-like properties by overexpressing a constitutively active the
333 Decapentaplegic (Dpp) receptor, Thickveins (Tkv.CA) in germline cells, or the
334 loss of function of *bag of marbles* (*bam*), a key differentiation factor
335 (Casanueva & Ferguson, 2004; D. Chen & McKearin, 2003a). These
336 manipulations resulted in the tumorigenic proliferation of undifferentiated
337 GSC-like cells or pre-cystoblast, respectively (Tiwari et al., 2019).
338 Remarkably, Tkv.CA overexpression and *bam* loss rescued germline cell
339 depletion in *stil* mutant ovaries, leading to the formation of tumorous germaria
340 containing undifferentiated germline cells comparable to the *stil* heterozygous
341 control (Fig. 5C, D). Indeed, TUNEL assay showed no increase in apoptotic
342 cells in such tumorous germaria (Fig. 5E, F), indicating that the
343 undifferentiated state of germline cells confers resistance to apoptosis in the
344 absence of *stil*.
345 Consistent with this observation, RNA-seq and gene Ontology (GO)
346 analysis of those tumorous ovaries revealed that the expression levels of
347 most apoptosis-related genes (GO:0006915), including *rpr*, remain unaffected
348 (PRJDB20709; Supplementary Table 2) (Fig. 5G). Furthermore, RT-qPCR

349 confirmed that *rpr* expression was not significantly upregulated in the GSC-
350 like tumor *stil* mutant ovaries compared to p35-rescued *stil* mutant ones (Fig.
351 3D, 5H), suggesting that apoptosis-related genes, including *rpr*, are
352 transcriptionally repressed in GSC-like cells even in the absence of *stil*
353 function.
354

355 **_rpr_ Silencing in Undifferentiated Germline Cells Is Associated with**
356 **Chromatin States**

357 Previous studies in mammals have established that stem cells are
358 generally resistant to apoptosis. In mouse mammary stem cells and cancer
359 stem cells, this resistance is attributed to several mechanisms, including
360 enhanced DNA repair and overexpression of anti-apoptotic proteins (Chang et
361 al., 2015; Nathansen et al., 2021; Safa, 2016). Similarly, in *Drosophila*,
362 intestinal stem cells were shown to resist cell death through a two-tiered
363 regulation of *rpr*, involving chromatin state and spatial control of its expression
364 (Sulekh et al., 2024). To explore whether chromatin dynamics contribute to
365 GSC apoptosis resistance in *stil* mutants, we analyzed the chromatin status at
366 the *rpr* locus using Assay for Transposase-Accessible Chromatin-seq (ATAC-
367 seq) data of Drosophila ovarian cells (Pang et al., 2023). This dataset was
368 generated using fluorescence-activated cell sorting (FACS) of GSCs (2C–4C)
369 and nurse cells (NCs) at various stages of egg chamber maturation, with
370 ploidy levels ranging from 4C to 512C due to endoreplication (Dej &
371 Spradling, 1999). In early mid-stage NCs where *stil* deficient-germline cells
372 undergo apoptosis, ATAC-seq signals were enriched at three upstream
373 regions of *rpr* (-0.5 to 0.5 kb, 1.5 to 2.0 kb, and 3.5 to 5.0 kb relative to the

374 transcription start site [TSS] of *rpr*) (Fig. 6A). Conversely, signals at these
375 three regions were significantly lower in 2C-4C GSCs and 64C-512C NCs.
376 These results suggest that the chromatin state upstream of *rpr* is closed in
377 GSCs and late-stage NCs (64C-512C) but open in early mid-stage NCs (4C-
378 32C). Notably, despite harboring the same ploidy, 4C GSCs and 4C NCs
379 displayed distinct chromatin accessibility, reflecting regulatory differences
380 likely responsible for their differential responses to apoptosis (Fig. 6A). We
381 further analyzed epigenetic marks such as H3K9me3 and H3K27me3 at the
382 *rpr* locus using publicly available data sets (DeLuca et al., 2020; Pang et al.,
383 2023). H3K9me3, a histone modification associated with transcriptional
384 repression, was observed around the *rpr* locus and its transcriptional control
385 region in GSCs, whereas only minimal signals were detected in 4C NCs (Fig.
386 6B). In contrast, H3K27me3, another repression mark exhibited no significant
387 difference between GSC and st5 NC (Fig. 6C) (DeLuca et al., 2020). This
388 suggests that H3K9me3, rather than H3K27me3, may establish a
389 heterochromatic state at the *rpr* loci in GSCs, contributing to transcriptional
390 silencing. These findings imply that chromatin dynamics play a crucial role in
391 regulating *rpr* expression during germline development.

392 **Discussion**

393 In this study, we investigated the role of the Drosophila gene *stand still* (*stil*),
394 which is required for the survival and maturation of female germline cells.
395 Loss of *stil* leads to apoptosis of germline cells via upregulation of the pro-
396 apoptotic gene *rpr* (Fig. 3E), identifying *rpr* as the primary effector of cell
397 death in this context. GFP-reporter assays with Stil variants in S2 cells
398 suggest that Stil represses *rpr* expression, likely through direct binding to its
399 upstream regulatory region via the BED-type zinc finger domain (Fig. 4H).

400 The transcription of *rpr* is regulated by multiple transcription factors
401 that bind to cis-regulatory elements located upstream of the gene (Fuchs &
402 Steller, 2011). For example, the tumor suppressor protein p53 binds to a well-
403 characterized p53 response element (p53RE) located 4.8 kb upstream of *rpr*,
404 which is responsive to intrinsic and extrinsic signals during embryogenesis
405 and in germline cells (Lu et al., 2010; Wylie et al., 2014). However, p53
406 binding to this element has only been observed in the anterior germarium, and
407 no direct link between p53 and apoptosis has been established in the female
408 germline (Park et al., 2019). Other known regulators, such as the homeobox
409 transcription factor Deformed (Dfd) and the JNK-responsive complex AP-1,
410 also bind upstream *rpr* enhancers in somatic tissues, but neither is active in
411 the female germline (Beira et al., 2014; Lohmann et al., 2002). Thus, factors
412 that suppress *rpr* transcription specifically in germline cells have remained
413 unidentified. Our study identifies Stil as a female germline-specific repressor

414 of *rpr*. DamID profiling revealed Stil binding to the *rpr* locus to 5–6 kb
415 upstream, covering regulatory elements associated with known transcription
416 factors (Fig. 4B). Consistently, Stil repressed *rpr*-GFP reporter containing the
417 5 kb upstream regulatory region in S2 cells, and this repression required Stil's
418 BED-type zinc finger domain (Fig. 4H). This domain is known to mediate DNA
419 binding and contribute to transcriptional regulation and chromatin remodeling
420 (Aravind, 2000). These findings support a model in which Stil directly occupies
421 the *rpr* regulatory region and blocks activator access to maintain
422 transcriptional repression in germline cells.

423 Whereas DIAP1 overexpression only partially rescued germline loss
424 in *stil* mutants, P35 restored germline survival in nearly all cases (Fig. 2G, H),
425 highlighting a functional distinction in how these inhibitors act in the context of
426 *rpr*-induced apoptosis. Both inhibit apoptosis through distinct mechanisms:
427 DIAP1 blocks caspase activation by inhibiting initiator and effector caspases,
428 while P35, a baculoviral protein, acts as a pseudo-substrate that irreversibly
429 inhibits effector caspases such as DrICE and Dcp-1 (Li et al., 2024; Nair &
430 Baker, 2024). *rpr* antagonizes DIAP1 through two independent mechanisms—
431 by promoting its auto-ubiquitination and proteasomal degradation, and by
432 inhibiting its translation (Freel et al., 2008; Holley et al., 2002). Therefore, high
433 *rpr* levels in *stil* mutant ovaries may deplete functional DIAP1, limiting the
434 rescue effect of its overexpression. By contrast, P35 directly targets
435 downstream caspases, bypassing DIAP1 loss and producing stronger

436 inhibition. These results support the model that Stil maintains the apoptotic
437 threshold by regulating *rpr* levels and balancing Rpr–DIAP1 interactions
438 (Sandu et al., 2010; Yin & Thummel, 2004).

439 Despite the loss of *stil*, undifferentiated female germline cells (GSCs
440 and pre-cyst cells) remain resistant to apoptosis (Fig. 5E, F), correlating with
441 closed chromatin and H3K9me3 enrichment at the *rpr* locus (Fig. 6A, B).
442 Similar chromatin-based repression of *rpr* has been reported in *Drosophila*
443 intestinal stem cells (Sulekh et al., 2024) and in late-stage embryos, where
444 heterochromatin silences *rpr* expression (Zhang et al., 2008). Together with
445 our findings, these studies suggest that chromatin-mediated silencing
446 provides an additional layer of protection against apoptosis in female GSCs,
447 independent of *stil*. By contrast, *stil* mutant male germline cells show no
448 phenotype and no *rpr* upregulation (Fig. S5B), suggesting that that rpr-
449 mediated apoptosis is not activated in the male germline. This points to a sex-
450 specific mechanism of *rpr* repression, potentially involving chromatin-based
451 silencing, although this possibility has yet to be examined.

452 Together, our findings reveal two mechanisms that protect female
453 germline cells from *rpr*-dependent apoptosis: Stil-mediated transcriptional
454 repression in differentiating germline cells and chromatin-based silencing in
455 undifferentiated germline cells. Although the upstream regulation of *stil* is
456 unknown, its selective role in female germline cells suggests it functions as a

457 developmental checkpoint that prevents premature apoptosis during

458 oogenesis. A key question is how *stil* integrates intrinsic or environmental

459 cues to modulate the apoptotic threshold during germline development.

460

461 ## Materials and Methods

462 ### Fly stock and cultures

463 All *Drosophila* stocks and crosses were reared at room temperature (25ºC) on
464 standard food [5% (w/v) dry yeast, 5% (w/v) corn flower, 2% (w/v) rice bran,
465 10% (w/v) glucose, 0.7% (w/v) agar, 0.2% (v/v) propionic acid and 0.05%
466 (w/v) p-hydroxy butyl benzoic acid]. The following stocks were used in this
467 study: *yellow white* (*y w)*, *attP2* (BL#25710), $stil^{EY16156}$ (BL#21191), $stil^{3}$
468 (BL#533, splicing donor site of the second intron was mutated from GTATG to
469 ATATG at 12570993), *Df(2R)vg-C* (BL#754, deficiency for *stil*), *Df(3L)X14*
470 (BL#600368, deficiency for *hid*) *UASp-P35* (a gift from Dr. Bergmann), *UASp-*
471 *DIAP1* (BL#63818), rpr^{87} (BL#83150), hid^{05014} (BL#83349), *UASp-Tkv.CA* (a
472 gift from Dr. Dahua Chen), $bam^{\Delta 86}$ (BL#5427), *NGT40-Gal4*; *nosGal4-VP16*
473 (Grieder et al., 2000), *mat* α*-tub-Gal4* (BL#7063), *bam-Gal4* (D. Chen &
474 McKearin, 2003b) , and *tj-Gal4* (DGRC#104055). The mutation site of $stil^{3}$
475 was identified by sanger sequencing of the PCR-amplified fragment.

476

477 ### Generation of transgenic fly lines

478 Transgenic fly lines expressing Stil variants (6×Myc-Stil-FL, 6×Myc-Stil-NT,
479 6×Myc-Stil-CT, and 6×Myc-Stil-AAYA) and DamID constructs (Dam-alone and
480 Dam-Stil) were generated using the PhiC31 integrase-mediated transgenesis
481 system. DNA fragments encoding Stil variant were amplified using cDNAs
482 obtained by reverse transcription of ovarian RNA extracted from *y w* flies.

483 DamID constructs were designed such that a primary open reading frame
484 (ORF) encoding GFP was followed by two stop codons and a secondary ORF
485 encoding either Dam or Dam-Stil (Southall et al., 2013). The DNA fragment
486 encoding Dam was amplified from the pUASTattB-LT3-NDam vector (a gift
487 from Dr. Andrea H. Brand). The resulting DNA fragments were cloned into the
488 pUASp-K10-attB plasmid backbone (Koch et al., 2009). These transgenic
489 constructs were injected into embryos of attP-containing strains (Stil variants
490 into P40, BDSC #25709, Dam and Dam-Stil into P2, BDSC #25710,
491 respectively), and transformants expressing *mini-white* were selected.

492

493 **Immunofluorescence staining**

494 Immunofluorescence staining was performed as previously described (Xu et
495 al., 2024). Ovaries and testis from adults and the 3rd instar larva were
496 dissected in cold phosphate buffer saline (PBS) and fixed with PBS containing
497 5.3% (w/v) paraformaldehyde for 10 min. Fixed samples were washed in PBX
498 [PBS with 0.2% (v/v) Triton-X (Nacalai)] for at least 30 min with several
499 change of solution, then blocked with PBX containing 4% (w/v) bovine serum
500 albumin (BSA) for at least 30 min at room temperature. After rinsing once with
501 PBX, the samples were incubated with the primary antibodies diluted in PBX
502 containing 0.4% (w/v) BSA for more than 4 h at room temperature or
503 overnight at 4ºC. After several washes with PBX for at least 1 h, the samples
504 were incubated in secondary antibodies diluted in PBX containing 0.4% (w/v)

505 BSA for more than 2 h at room temperature. The samples were washed
506 several times with PBX for at least 1 h and stained with 1 μg/ml of 4',6-
507 diamidino-2phenylindole (DAPI) (Sigma) diluted in PBX for 10 min at room
508 temperature. Following two rinses with PBX and PBS, tissues were mounted
509 in Fluoro-KEEPER Antifade Reagent (Nacalai). The following primary
510 antibodies were used at the indicated dilutions: guinea pig anti-Vas (1:1000)
511 (Patil & Kai, 2010), mouse anti c-Myc [Wako (9E10), 1:500], and rabbit anti-
512 FLAG [MBL, PM020, 1:1000]. Secondary antibodies were Alexa Fluor 488-
513 and 555-conjugated goat antibodies against rabbit, mouse and guinea pig IgG
514 (Invitrogen, A11029, A11034, A11073, A21424, A21429 and A21435) at a
515 1:200 dilution in PBX containing 0.4% (w/v) BSA. Images were captured by
516 Zeiss LSM780 Confocal Microscope with 10x, 20x, and 40x lens and
517 processed with Zen (Zeiss) and Fiji application (Schindelin et al., 2012) .

518

519 **TUNEL assay**

520 TUNEL assay was conducted using ApopTag® Kits (Millipore), labelling the
521 free 3'-OH DNA termini in situ with fluorescein-nucleotide by terminal
522 deoxynucleotidyl transferase (TdT). Dissected ovaries in cold PBS were fixed
523 with PBS containing 5.3% (w/v) paraformaldehyde and rinsed 3 times with
524 PBX. Ovaries were washed with PBX for 10 min twice and further washed
525 with PBST [PBS with 0.1% (v/v) Tween 20 (Nacalai)] twice. After rinsing with
526 Equilibration Buffer twice, the samples were incubated with TdT reagent [70%

527 (v/v) Reaction Buffer and 30% (v/v) TdT Enzyme] for 1 h at 37ºC. After
528 incubation with 1/35 diluted Stop/Wash Buffer for 15 min, samples were
529 rinsed 3 times with PBX and then washed 3 times with PBX for 10 min. The
530 tissue mounting and microscopic observation were as described in the
531 "Immunofluorescence staining" section.

532

533 **RT-PCR and quantitative RT-PCR**

534 Total RNA was isolated from ovaries using TRIzol LS Reagent (Invitrogen),
535 following the manufacturer's protocol. RNA samples (1 µg each) were treated
536 with DNase I (NEB) to digest genomic DNA, followed by inactivation of the
537 enzyme with 5 mM EDTA at 75ºC for 10 min. Reverse transcription was
538 performed using the DNase I-treated RNA with oligo(dT)20 primers and
539 SuperScript III Reverse Transcriptase (Invitrogen), following the
540 manufacturer's protocol. cDNAs were subjected to 30 cycles of RT-PCR with
541 GoTaq DNA polymerase (Promega).

542 Quantitative PCR (qPCR) was performed with Fast SYBR Green regents
543 (Invitrogen) using at least 3 biological replicates. Deltal-delta-CT method was
544 used to obtain the relative transcript levels. *α-Tub84B (tubulin)* was used as
545 the reference. The sequences of the primers are listed in Supplementary
546 Table 3.

547

548 **mRNA-seq analysis**

549 Total RNAs were extracted from 100 ovaries of control and *stil* mutant of
550 *Tkv.CA OE* background and 40 ovaries of control and *stil* mutant of *P35 OE*
551 background using TRIzol (ThermoFisher) following the manufacture's
552 instruction. Extracted RNAs were treated with DNase I for 10 min at 37ºC and
553 reactions were inhibited by 5 mM EDTA at 70ºC for 10 min, following that
554 RNAs were purified using phenol/ chloroform/ isoamyl alcohol (mixed with a
555 ratio of 25: 24: 1, pH 5.2). Purified RNAs were prepared for mRNA-seq
556 libraries with NEBNext Ultra II RNA Library Prep Kit for Illumina (NEB), and
557 deep-sequencing was conducted using NovaSeq6000 (Illumina). Sequencing
558 analysis was conducted using bioinformatic software, CLC workbench 12
559 (QIAGEN). Adaptor sequences of total reads obtained from mRNA-seq were
560 trimmed and reads were mapped to *Drosophila* genomes, r6.32 from Flybase
561 (ftp://ftp.flybase.net/genomes/Drosophila_melanogaster/). After mapping the
562 sequence data, Differential expression analysis was performed between
563 control and *stil* mutant with *P35 OE* or*Tkv.CA OE* and calculated the
564 expression level of each gene.

565

566 **DamID-seq and data processing**

567 UASp-Dam and UASp-Dam-Stil flies were crossed with *NGT40; NosGal4-*
568 *VP16* driver and maintained at 25°C. For each replicate, 100 ovaries of 50
569 flies were dissected in *Drosophila* Schneider's medium. Genomic DNA was
570 extracted using the QIAamp Fast DNA Tissue Kit (QIAGEN cat. no. 51404),
571 and methylated DNA was processed and amplified as described (Díaz-Torres
572 et al., 2021). Briefly, genomic DNA was digested overnight with *Dpn*I (NEB),
573 which cuts methylated GATC sites, and DamID adaptors were ligated to the
574 resulting fragments. A subsequent digestion with *Dpn*II (NEB), which
575 selectively cuts unmethylated GATC sites, was performed, and fragments
576 containing consecutive methylated GATCs were then amplified by PCR using
577 ligated adaptor-specific primers and PrimeSTAR® HS DNA Polymerase
578 (Takara).

579 The amplified DNA was sonicated using a Bioruptor (Diagenode) to obtain an
580 average fragment size of 300 bp. DamID adaptors were removed by digestion
581 with *Alw*I, and the DNA was purified using AMPure XP beads (Beckman
582 Coulter). For next-generation sequencing, the DNA was subjected to end-
583 repair, A-tailing, Illumina adaptor ligation, and PCR amplification. Single-end
584 100 bp reads were subsequently generated on a NovaSeq 6000 platform
585 (Illumina). Illumina NGS reads were aligned to the *Drosophila melanogaster*
586 reference genome (r6.32), and enrichment profiles were generated using the
587 damidseq_pipeline with default settings (Marshall & Brand, 2015), with
588 replicate libraries subsequently averaged. The Dam-Stil enrichment profile

589 was normalized by the Dam control profile and Dam-Stil peaks were identified
590 using find_peaks and annotated with the ChIPseeker pipeline (Marshall &
591 Brand, 2015) .

592

593 **Fertility test**

594 For female fertility assays, three virgin females were mated with three *y w*
595 males for 3 days per replicate. For male fertility assays, three males were
596 mated with three *y w* virgin females under the same conditions. After the
597 mating period, eggs were collected for 24 hours, followed by incubation for an
598 additional 24 hours. The total number of eggs and the number of hatched
599 eggs were then counted for each replicate.

600

601 **S2 cell culture experiments**

602 *Drosophila* Schneider S2 cells were cultured at 28°C in Schneider's medium
603 (Thermo) supplemented with 10% (v/v) fetal bovine serum (FBS), 100 U/mL
604 penicillin, and 100 µg/mL streptomycin (Thermo). Plasmids encoding Stil
605 variants were generated using the Gateway cloning system with (Life
606 Technologies) with pAFW, which drives the expression of N-terminal FLAG-
607 tagged fusion proteins under the control of the Actin5C promoter. *rpr*-GFP

608 reporter plasmid was constructed by replacing 2.4-kb tubulin promoter of
609 the *tubP*-GFP, a gift from Dr, Steve Cohen (Brennecke et al., 2003), with the
610 PCR-amplified 5 kb promoter region of *rpr*.

611 For the reporter assay, a total of 4 μg of plasmid DNA was used for each
612 transfection. Transgenes and reporter plasmids were included at 1 μg each as
613 needed, and the remaining amount was supplemented with the control
614 plasmid pAW without attR sites to reach 4 μg. The plasmid mixture was
615 combined with 20 μL of Hilymax transfection reagent (Dojindo) and
616 transfected into 1 mL of S2 cells seeded one day prior, following the
617 manufacturer's instructions. Two days of post-transfection, cells were
618 collected, sonicated, and followed by centrifugation. The supernatant was
619 mixed with 20% volume of 5× sample buffer. Proteins were then analyzed by
620 Western blotting using the following antibodies and Signal Enhancer Reagent
621 HIKARI (Nacalai): mouse anti-α-Tubulin [Santa Cruz, DM1A, 1:1000] rabbit
622 anti-GFP [Clonetech, 632569, 1:1000], and rabbit anti-FLAG [MBL, PM020,
623 1:1000]. Chemiluminescence detection was performed using the Chemi-Lumi
624 One reagent kit (Nacalai), and immunoreactive bands were visualized with a
625 ChemiDoc Touch imaging system (Bio-Rad) and analyzed using Fiji
626 (Schindelin et al., 2012).

627 For immunostaining, transfected S2 cells were collected at 2-days post-
628 transfection and plated onto poly-L-Lysine-coated coverslips for at least 30

629 min to promote adhesion. Cells were fixed in 5.3% (w/v) paraformaldehyde for
630 15 min, permeabilized with PBX for 10 min, and washed three times with
631 PBX. After blocking with PBX containing 4% (w/v) BSA for 30 min, cells were
632 incubated with primary and secondary antibodies for at least 1 hour each,
633 followed by nuclear staining with 1 μg/ml of DAPI for 10 min. After rinsing with
634 PBS, samples were mounted with Fluoro-KEEPER Antifade Reagent
635 (Nacalai). Images were acquired using a Zeiss LSM780 and 900 confocal
636 microscopes with a 63× objective lens and processed using Zen and ImageJ
637 software.

638

Competing Interest Statement

The authors declare that the research was conducted in the absence of any commercial or financial relationships that could be construed as a potential conflict of interest.

Acknowledgments

We thank Dr. Andrea H. Brand (The Gurdon Institute, University of Cambridge), Dr. Andreas Bergmann (UMass Chan Medical School, Massachusetts), and Dr. Dahua Chen (Yunnan University Institute of Biomedical Research, Kunming) for their generous gifts of the Dam CDS plasmid, the UASp-P35 transgenic fly line, and the UASp-Tkv.CA transgenic fly line, respectively. We acknowledge Bloomington Drosophila Stock Centre for the fly stocks. Confocal images and Western blotting data were acquired with LSM780, LSM900 and ChemiDoc Touch, respectively, at FBS Core Facility in The University of Osaka. We appreciate the insightful discussion and suggestions from all the members of KT's laboratory.

Author Contributions

All authors contributed to the experiment design. MM, KS, and KT performed all experiments. MM and KS performed the computational analyses. MM, KS, and KT wrote the paper. KS and KT supervised the project.

661 ## References

662 Abbott, M. K. & Lengyel, J. A. (1991). Embryonic head involution and rotation
663 of male terminalia require the Drosophila locus head involution defective.
664 *Genetics*, *129*(3), 783–789. https://doi.org/10.1093/genetics/129.3.783

665 Almeida, C., Correia, S., Rocha, E., Alves, Â., Ferraz, L., Silva, J., Sousa, M.
666 & Barros, A. (2013). Caspase signalling pathways in human
667 spermatogenesis. *Journal of Assisted Reproduction and Genetics*, *30*(4),
668 487–495. https://doi.org/10.1007/s10815-013-9938-8

669 Aravind, L. (2000). The BED finger, a novel DNA-binding domain in
670 chromatin-boundary-element-binding proteins and transposases. *Trends in*
671 *Biochemical Sciences*, *25*(9), 421–423. https://doi.org/10.1016/s0968-
672 0004(00)01620-0

673 Aughey, G. N., Cheetham, S. W. & Southall, T. D. (2019). DamID as a
674 versatile tool for understanding gene regulation. *Development*, *146*(6),
675 dev173666. https://doi.org/10.1242/dev.173666

676 Baonza, A., Tur-Gracia, S., Pérez-Aguilera, M. & Estella, C. (2022).
677 Regulation and coordination of the different DNA damage responses in
678 Drosophila. *Frontiers in Cell and Developmental Biology*, *10*, 993257.
679 https://doi.org/10.3389/fcell.2022.993257

680 Baum, J. S., Arama, E., Steller, H. & McCall, K. (2007). The Drosophila
681 caspases Strica and Dronc function redundantly in programmed cell death
682 during oogenesis. *Cell Death & Differentiation*, *14*(8), 1508–1517.
683 https://doi.org/10.1038/sj.cdd.4402155

684 Beira, J. V., Springhorn, A., Gunther, S., Hufnagel, L., Pyrowolakis, G. &
685 Vincent, J.-P. (2014). The Dpp/TGFβ-Dependent Corepressor Schnurri
686 Protects Epithelial Cells from JNK-Induced Apoptosis in Drosophila
687 Embryos. *Developmental Cell*, *31*(2), 240–247.
688 https://doi.org/10.1016/j.devcel.2014.08.015

689 Bell, L. R., Horabin, J. I., Schedl, P. & Cline, T. W. (1991). Positive
690 autoregulation of Sex-lethal by alternative splicing maintains the female
691 determined state in Drosophila. *Cell*, *65*(2), 229–239.
692 https://doi.org/10.1016/0092-8674(91)90157-t

693 Bellen, H. J., Levis, R. W., He, Y., Carlson, J. W., Evans-Holm, M., Bae, E.,
694 Kim, J., Metaxakis, A., Savakis, C., Schulze, K. L., Hoskins, R. A. &
695 Spradling, A. C. (2011). The Drosophila Gene Disruption Project: Progress

696 Using Transposons With Distinctive Site Specificities. *Genetics*, *188*(3),
697 731–743. https://doi.org/10.1534/genetics.111.126995

698 Bellen, H. J., Levis, R. W., Liao, G., He, Y., Carlson, J. W., Tsang, G., Evans-
699 Holm, M., Hiesinger, P. R., Schulze, K. L., Rubin, G. M., Hoskins, R. A. &
700 Spradling, A. C. (2004). The BDGP Gene Disruption Project. *Genetics*,
701 *167*(2), 761–781. https://doi.org/10.1534/genetics.104.026427

702 Brennecke, J., Hipfner, D. R., Stark, A., Russell, R. B. & Cohen, S. M. (2003).
703 bantam Encodes a Developmentally Regulated microRNA that Controls
704 Cell Proliferation and Regulates the Proapoptotic Gene hid in Drosophila.
705 *Cell*, *113*(1), 25–36. https://doi.org/10.1016/s0092-8674(03)00231-9

706 Brodsky, M. H., Nordstrom, W., Tsang, G., Kwan, E., Rubin, G. M. & Abrams,
707 J. M. (2000). Drosophila p53 Binds a Damage Response Element at the
708 reaper Locus. *Cell*, *101*(1), 103–113. https://doi.org/10.1016/s0092-
709 8674(00)80627-3

710 Casanueva, M. O. & Ferguson, E. L. (2004). Germline stem cell number in the
711 Drosophila ovary is regulated by redundant mechanisms that control Dpp
712 signaling. *Development*, *131*(9), 1881–1890.
713 https://doi.org/10.1242/dev.01076

714 Chang, C.-H., Zhang, M., Rajapakshe, K., Coarfa, C., Edwards, D., Huang, S.
715 & Rosen, J. M. (2015). Mammary Stem Cells and Tumor-Initiating Cells Are
716 More Resistant to Apoptosis and Exhibit Increased DNA Repair Activity in
717 Response to DNA Damage. *Stem Cell Reports*, *5*(3), 378–391.
718 https://doi.org/10.1016/j.stemcr.2015.07.009

719 Chaudhry, S. R., Lopes, J., Levin, N. K., Kalpage, H. & Tainsky, M. A. (2021).
720 Germline mutations in apoptosis pathway genes in ovarian cancer; the
721 functional role of a TP53I3 (PIG3) variant in ROS production and DNA
722 repair. *Cell Death Discovery*, *7*(1), 62. https://doi.org/10.1038/s41420-021-
723 00442-y

724 Chen, D. & McKearin, D. (2003a). Dpp Signaling Silences bam Transcription
725 Directly to Establish Asymmetric Divisions of Germline Stem Cells. *Current*
726 *Biology*, *13*(20), 1786–1791. https://doi.org/10.1016/j.cub.2003.09.033

727 Chen, D. & McKearin, D. M. (2003b). A discrete transcriptional silencer in the
728 bam gene determines asymmetric division of the Drosophila germline stem
729 cell. *Development*, *130*(6), 1159–1170. https://doi.org/10.1242/dev.00325

730 Chen, P., Nordstrom, W., Gish, B. & Abrams, J. M. (1996). grim, a novel cell
731 death gene in Drosophila. *Current Biology*, *6*(7), 767.
732 https://doi.org/10.1016/s0960-9822(02)00588-2

733 Christich, A., Kauppila, S., Chen, P., Sogame, N., Ho, S.-I. & Abrams, J. M.
734 (2002). The Damage-Responsive Drosophila Gene sickle Encodes a Novel
735 IAP Binding Protein Similar to but Distinct from reaper, grim, and hid.
736 *Current Biology*, *12*(2), 137–140. https://doi.org/10.1016/s0960-
737 9822(01)00658-3

738 Dej, K. J. & Spradling, A. C. (1999). The endocycle controls nurse cell
739 polytene chromosome structure during Drosophila oogenesis.
740 *Development*, *126*(2), 293–303. https://doi.org/10.1242/dev.126.2.293

741 DeLuca, S. Z., Ghildiyal, M., Pang, L.-Y. & Spradling, A. C. (2020).
742 Differentiating Drosophila female germ cells initiate Polycomb silencing by
743 regulating PRC2-interacting proteins. *ELife*, *9*, e56922.
744 https://doi.org/10.7554/elife.56922

745 Díaz-Torres, A., Rosales-Nieves, A. E., Pearson, J. R., Mateos, C. S.-C.,
746 Marín-Menguiano, M., Marshall, O. J., Brand, A. H. & González-Reyes, A.
747 (2021). Stem cell niche organization in the Drosophila ovary requires the
748 ECM component Perlecan. *Current Biology*, *31*(8), 1744-1753.e5.
749 https://doi.org/10.1016/j.cub.2021.01.071

750 Drummond-Barbosa, D. & Spradling, A. C. (2001). Stem Cells and Their
751 Progeny Respond to Nutritional Changes during Drosophila Oogenesis.
752 *Developmental Biology*, *231*(1), 265–278.
753 https://doi.org/10.1006/dbio.2000.0135

754 Freel, C. D., Richardson, D. A., Thomenius, M. J., Gan, E. C., Horn, S. R.,
755 Olson, M. R. & Kornbluth, S. (2008). Mitochondrial Localization of Reaper
756 to Promote Inhibitors of Apoptosis Protein Degradation Conferred by GH3
757 Domain-Lipid Interactions*. *Journal of Biological Chemistry*, *283*(1), 367–
758 379. https://doi.org/10.1074/jbc.m708931200

759 Fuchs, Y. & Steller, H. (2011). Programmed Cell Death in Animal
760 Development and Disease. *Cell*, *147*(4), 742–758.
761 https://doi.org/10.1016/j.cell.2011.10.033

762 Fuchs, Y. & Steller, H. (2015). Live to die another way: modes of programmed
763 cell death and the signals emanating from dying cells. *Nature Reviews*
764 *Molecular Cell Biology*, *16*(6), 329–344. https://doi.org/10.1038/nrm3999

765 G, P. & D., P. (1997). stand still, a Drosophila gene involved in the female
766 germline for proper survival, sex determination and differentiation.
767 *Genetics*, *145*(4), 975–987. https://doi.org/10.1093/genetics/145.4.975

768 Gleason, R. J., Anand, A., Kai, T. & Chen, X. (2018). Protecting and
769 Diversifying the Germline. *Genetics*, *208*(2), 435–471.
770 https://doi.org/10.1534/genetics.117.300208

771 Grieder, N. C., Cuevas, M. de & Spradling, A. C. (2000). The fusome
772 organizes the microtubule network during oocyte differentiation in
773 Drosophila. *Development*, *127*(19), 4253–4264.
774 https://doi.org/10.1242/dev.127.19.4253

775 Hashiyama, K., Hayashi, Y. & Kobayashi, S. (2011). Drosophila Sex lethal
776 Gene Initiates Female Development in Germline Progenitors. *Science*,
777 *333*(6044), 885–888. https://doi.org/10.1126/science.1208146

778 Holley, C. L., Olson, M. R., Colón-Ramos, D. A. & Kornbluth, S. (2002).
779 Reaper eliminates IAP proteins through stimulated IAP degradation and
780 generalized translational inhibition. *Nature Cell Biology*, *4*(6), 439–444.
781 https://doi.org/10.1038/ncb798

782 Hou, Y.-C. C., Chittaranjan, S., Barbosa, S. G., McCall, K. & Gorski, S. M.
783 (2008). Effector caspase Dcp-1 and IAP protein Bruce regulate starvation-
784 induced autophagy during Drosophila melanogaster oogenesis. *The*
785 *Journal of Cell Biology*, *182*(6), 1127–1139.
786 https://doi.org/10.1083/jcb.200712091

787 Huang, C., Zhao, S., Yang, Y., Guo, T., Ke, H., Mi, X., Qin, Y., Chen, Z.-J. &
788 Zhao, S. (2023). TP63 gain-of-function mutations cause premature ovarian
789 insufficiency by inducing oocyte apoptosis. *Journal of Clinical Investigation*,
790 *133*(5), e162315. https://doi.org/10.1172/jci162315

791 Jiang, C., Lamblin, A.-F. J., Steller, H. & Thummel, C. S. (2000). A Steroid-
792 Triggered Transcriptional Hierarchy Controls Salivary Gland Cell Death
793 during Drosophila Metamorphosis. *Molecular Cell*, *5*(3), 445–455.
794 https://doi.org/10.1016/s1097-2765(00)80439-6

795 Knudson, C. M., Tung, K. S. K., Tourtellotte, W. G., Brown, G. A. J. &
796 Korsmeyer, S. J. (1995). Bax-Deficient Mice with Lymphoid Hyperplasia
797 and Male Germ Cell Death. *Science*, *270*(5233), 96–99.
798 https://doi.org/10.1126/science.270.5233.96

799 Koch, R., Ledermann, R., Urwyler, O., Heller, M. & Suter, B. (2009).
800 Systematic Functional Analysis of Bicaudal-D Serine Phosphorylation and

801 Intragenic Suppression of a Female Sterile Allele of BicD. *PLoS ONE*, *4*(2),
802 e4552. https://doi.org/10.1371/journal.pone.0004552

803 Li, J., Jordana, L., Mehsen, H., Wang, X. & Archambault, V. (2024). Nuclear
804 reassembly defects after mitosis trigger apoptotic and p53-dependent
805 safeguard mechanisms in Drosophila. *PLOS Biology*, *22*(8), e3002780.
806 https://doi.org/10.1371/journal.pbio.3002780

807 Lohmann, I., McGinnis, N., Bodmer, M. & McGinnis, W. (2002). The
808 Drosophila Hox Gene Deformed Sculpts Head Morphology via Direct
809 Regulation of the Apoptosis Activator reaper. *Cell*, *110*(4), 457–466.
810 https://doi.org/10.1016/s0092-8674(02)00871-1

811 Lu, W.-J., Chapo, J., Roig, I. & Abrams, J. M. (2010). Meiotic Recombination
812 Provokes Functional Activation of the p53 Regulatory Network. *Science*,
813 *328*(5983), 1278–1281. https://doi.org/10.1126/science.1185640

814 Marshall, O. J. & Brand, A. H. (2015). damidseq_pipeline: an automated
815 pipeline for processing DamID sequencing datasets. *Bioinformatics*,
816 *31*(20), 3371–3373. https://doi.org/10.1093/bioinformatics/btv386

817 McCall, K. (2004). Eggs over easy: cell death in the Drosophila ovary.
818 *Developmental Biology*, *274*(1), 3–14.
819 https://doi.org/10.1016/j.ydbio.2004.07.017

820 McKowen, J. K., Avva, S. V. S. P., Maharjan, M., Duarte, F. M., Tome, J. M.,
821 Judd, J., Wood, J. L., Negedu, S., Dong, Y., Lis, J. T. & Hart, C. M. (2022).
822 The Drosophila BEAF insulator protein interacts with the polybromo subunit
823 of the PBAP chromatin remodeling complex. *G3*, *12*(11), jkac223.
824 https://doi.org/10.1093/g3journal/jkac223

825 Moschall, R., Rass, M., Rossbach, O., Lehmann, G., Kullmann, L., Eichner,
826 N., Strauss, D., Meister, G., Schneuwly, S., Krahn, M. P. & Medenbach, J.
827 (2019). Drosophila Sister-of-Sex-lethal reinforces a male-specific gene
828 expression pattern by controlling Sex-lethal alternative splicing. *Nucleic*
829 *Acids Research*, *47*(5), 2276–2288. https://doi.org/10.1093/nar/gky1284

830 Nair, S. & Baker, N. E. (2024). Extramacrochaetae regulates Notch signaling
831 in the Drosophila eye through non-apoptotic caspase activity. *ELife*, *12*,
832 RP91988. https://doi.org/10.7554/elife.91988

833 Nathansen, J., Meyer, F., Müller, L., Schmitz, M., Borgmann, K. & Dubrovska,
834 A. (2021). Beyond the Double-Strand Breaks: The Role of DNA Repair
835 Proteins in Cancer Stem-Cell Regulation. *Cancers*, *13*(19), 4818.
836 https://doi.org/10.3390/cancers13194818

837 Pang, L.-Y., DeLuca, S., Zhu, H., Urban, J. M. & Spradling, A. C. (2023).
838 Chromatin and gene expression changes during female Drosophila
839 germline stem cell development illuminate the biology of highly potent stem
840 cells. *ELife*, *12*(6), RP90509. https://doi.org/10.7554/elife.90509

841 Park, J.-H., Nguyen, T. T. N., Lee, E.-M., Castro-Aceituno, V., Wagle, R., Lee,
842 K.-S., Choi, J. & Song, Y.-H. (2019). Role of p53 isoforms in the DNA
843 damage response during Drosophila oogenesis. *Scientific Reports*, *9*(1),
844 11473. https://doi.org/10.1038/s41598-019-47913-y

845 Patil, V. S. & Kai, T. (2010). Repression of Retroelements in Drosophila
846 Germline via piRNA Pathway by the Tudor Domain Protein Tejas. *Current*
847 *Biology*, *20*(8), 724–730. https://doi.org/10.1016/j.cub.2010.02.046

848 Peterson, Jeanne S., Bass, B. P., Jue, D., Rodriguez, A., Abrams, J. M. &
849 McCall, K. (2007). Noncanonical cell death pathways act during Drosophila
850 oogenesis. *Genesis*, *45*(6), 396–404. https://doi.org/10.1002/dvg.20306

851 Peterson, J.S, Barkett, M. & McCall, K. (2003). Stage-specific regulation of
852 caspase activity in drosophila oogenesis. *Developmental Biology*, *260*(1),
853 113–123. https://doi.org/10.1016/s0012-1606(03)00240-9

854 PK, M., AR, C. & JR, J. (1996). Mutations in the gene stand still disrupt germ
855 cell differentiation in Drosophila ovaries. *Developmental Genetics*, *18*(4),
856 316–324. https://doi.org/10.1002/(sici)1520-6408(1996)18:4<316::aid-
857 dvg5>3.0.co;2-c

858 Primus, S., Pozmanter, C., Baxter, K. & Doren, M. V. (2019). Tudor-domain
859 containing protein 5-like promotes male sexual identity in the Drosophila
860 germline and is repressed in females by Sex lethal. *PLoS Genetics*, *15*(7),
861 e1007617. https://doi.org/10.1371/journal.pgen.1007617

862 Pritchett, T L & McCall, K. (2012). Role of the insulin/Tor signaling network in
863 starvation-induced programmed cell death in Drosophila oogenesis. *Cell*
864 *Death & Differentiation*, *19*(6), 1069–1079.
865 https://doi.org/10.1038/cdd.2011.200

866 Pritchett, Tracy L., Tanner, E. A. & McCall, K. (2009). Cracking open cell
867 death in the Drosophila ovary. *Apoptosis*, *14*(8), 969.
868 https://doi.org/10.1007/s10495-009-0369-z

869 Safa, A. R. (2016). Resistance to Cell Death and Its Modulation in Cancer
870 Stem Cells. *Critical Reviews in Oncogenesis*, *21*(3–4), 203–219.
871 https://doi.org/10.1615/critrevoncog.2016016976

872 Sahut-Barnola, I. & Pauli, D. (1999). The Drosophila gene stand still encodes
873 a germline chromatin-associated protein that controls the transcription of
874 the ovarian tumor gene. *Development*, *126*(9), 1917–1926.
875 https://doi.org/10.1242/dev.126.9.1917

876 Sandu, C., Ryoo, H. D. & Steller, H. (2010). Drosophila IAP antagonists form
877 multimeric complexes to promote cell death. *Journal of Cell Biology*,
878 *190*(6), 1039–1052. https://doi.org/10.1083/jcb.201004086

879 Schindelin, J., Arganda-Carreras, I., Frise, E., Kaynig, V., Longair, M.,
880 Pietzsch, T., Preibisch, S., Rueden, C., Saalfeld, S., Schmid, B., Tinevez,
881 J.-Y., White, D. J., Hartenstein, V., Eliceiri, K., Tomancak, P. & Cardona, A.
882 (2012). Fiji: an open-source platform for biological-image analysis. *Nature*
883 *Methods*, *9*(7), 676–682. https://doi.org/10.1038/nmeth.2019

884 Schüpbach, T. & Wieschaus, E. (1989). Female sterile mutations on the
885 second chromosome of Drosophila melanogaster. I. Maternal effect
886 mutations. *Genetics*, *121*(1), 101–117.
887 https://doi.org/10.1093/genetics/121.1.101

888 Sokolova, O., Morgunova, V., Sizova, T. V., Komarov, P. A., Olenkina, O. M.,
889 Babaev, D. S., Mikhaleva, E. A., Kwon, D. A., Erokhin, M. & Kalmykova, A.
890 (2023). The insulator BEAF32 controls the spatial-temporal expression
891 profile of the telomeric retrotransposon TART in the Drosophila germline.
892 *Development*, *150*(12). https://doi.org/10.1242/dev.201678

893 Southall, T. D., Gold, K. S., Egger, B., Davidson, C. M., Caygill, E. E.,
894 Marshall, O. J. & Brand, A. H. (2013). Cell-Type-Specific Profiling of Gene
895 Expression and Chromatin Binding without Cell Isolation: Assaying RNA
896 Pol II Occupancy in Neural Stem Cells. *Developmental Cell*, *26*(1), 101–
897 112. https://doi.org/10.1016/j.devcel.2013.05.020

898 Spradling, A., Drummond-Barbosa, D. & Kai, T. (2001). Stem cells find their
899 niche. *Nature*, *414*(6859), 98–104. https://doi.org/10.1038/35102160

900 Sulekh, S., Ikegawa, Y., Naito, S., Oji, A., Hiratani, I. & Yoo, S. K. (2024). A
901 feedback loop that drives cell death and proliferation and its defect in
902 intestinal stem cells. *Life Science Alliance*, *7*(4), e202302238.
903 https://doi.org/10.26508/lsa.202302238

904 Tiwari, M. D., Zeitler, D. M., Meister, G. & Wodarz, A. (2019). Molecular
905 profiling of stem cell-like female germ line cells in Drosophila delineates
906 networks important for stemness and differentiation. *Biology Open*, *8*(11),
907 bio046789. https://doi.org/10.1242/bio.046789

908 Tue, N. T., Yoshioka, Y., Mizoguchi, M., Yoshida, H., Zurita, M. & Yamaguchi,
909 M. (2017). DREF plays multiple roles during Drosophila development.
910 *Biochimica et Biophysica Acta (BBA) - Gene Regulatory Mechanisms*,
911 *1860*(6), 705–712. https://doi.org/10.1016/j.bbagrm.2017.03.004

912 Werz, C., Lee, T. V., Lee, P. L., Lackey, M., Bolduc, C., Stein, D. S. &
913 Bergmann, A. (2005). Mis-specified cells die by an active gene-directed
914 process, and inhibition of this death results in cell fate transformation in
915 Drosophila. *Development*, *132*(24), 5343–5352.
916 https://doi.org/10.1242/dev.02150

917 White, K., Grether, M. E., Abrams, J. M., Young, L., Farrell, K. & Steller, H.
918 (1994). Genetic Control of Programmed Cell Death in Drosophila. *Science*,
919 *264*(5159), 677–683. https://doi.org/10.1126/science.8171319

920 Wylie, A., Lu, W.-J., D'Brot, A., Buszczak, M. & Abrams, J. M. (2014). p53
921 activity is selectively licensed in the Drosophila stem cell compartment.
922 *ELife*, *3*, e01530. https://doi.org/10.7554/elife.01530

923 Xing, Y., Su, T. T. & Ruohola-Baker, H. (2015). Tie-mediated signal from
924 apoptotic cells protects stem cells in Drosophila melanogaster. *Nature*
925 *Communications*, *6*(1), 7058. https://doi.org/10.1038/ncomms8058

926 Xu, F., Suyama, R., Inada, T., Kawaguchi, S. & Kai, T. (2024). HemK2
927 functions for sufficient protein synthesis and RNA stability through eRF1
928 methylation during Drosophila oogenesis. *Development*, *151*(14).
929 https://doi.org/10.1242/dev.202795

930 Yan, N., Wu, J.-W., Chai, J., Li, W. & Shi, Y. (2004). Molecular mechanisms of
931 DrICE inhibition by DIAP1 and removal of inhibition by Reaper, Hid and
932 Grim. *Nature Structural & Molecular Biology*, *11*(5), 420–428.
933 https://doi.org/10.1038/nsmb764

934 Yin, V. P. & Thummel, C. S. (2004). A balance between the diap1 death
935 inhibitor and reaper and hid death inducers controls steroid-triggered cell
936 death in Drosophila. *Proceedings of the National Academy of Sciences*,
937 *101*(21), 8022–8027. https://doi.org/10.1073/pnas.0402647101

938 Zhang, Y., Lin, N., Carroll, P. M., Chan, G., Guan, B., Xiao, H., Yao, B., Wu,
939 S. S. & Zhou, L. (2008). Epigenetic Blocking of an Enhancer Region
940 Controls Irradiation-Induced Proapoptotic Gene Expression in Drosophila
941 Embryos. *Developmental Cell*, *14*(4), 481–493.
942 https://doi.org/10.1016/j.devcel.2008.01.018

943

944 ## Legends

945 **Figure 1. Disruption of *stil* induces female germline cell depletion**

946 (A) Schematic representation of the *Drosophila stil* gene locus showing the
947 position of P-element insertion, *EY16156*, mutation site of $stil^3$, and the target
948 site of shRNA for knockdown. Black and blue arrows represent primers for RT-
949 PCR and RT-qPCR, respectively. (B) Expression of *stil* and the control *α-tub*
950 transcripts in $stil^{EY16156}$ mutant and the heterozygous control ovaries or testes
951 analyzed by RT-PCR. (C) Representative images showing entire ovarian
952 morphology (left panels) and ovarioles immunostained with with a germline
953 marker, Vasa (red), and nuclear staining with DAPI (blue) (right panels) from *y*
954 *w*, $stil^{EY16156}/CyO$, $stil^{EY16156}$, $stil^{EY16156}/Df$, and $stil^{EY16156}$ expressing *6×Myc-Stil-*
955 *FL* transgene driven by the germline-specific driver, *NGT40; NosGal4-VP16*.
956 Scale bar: 1 mm for whole ovaries in the left panels, 50 μm for ovariole in the
957 right panels. (D) Quantification of the percentage of germline cell-containing
958 ovarioles in 2-3-days old females. Genotypes are indicated below the graph
959 and the numbers of ovarioles assessed are shown above each bar. Error bars
960 represent standard deviation (s.d.). (E) Analysis of egg laying and hatching rate.
961 The egg numbers and their hatching rate by three females indicated genotypes
962 corresponding to those in (C) mated with three *y w* males were measured daily
963 (*n*=3). Error bars indicate s.d.

964 **Figure 2. *stil* loss induces apoptotic cell death in female germline cells**

965 (A) Quantitative RT-PCR confirming the knockdown efficiency in ovaries of *stil*-
966 germline knockdown (*stil*-GLKD) where shRNA targeting stil transcript was
967 driven by *NGT40; NosGal4-VP16*, and the control with shRNA alone.
968 Expression levels of an internal control, *rp49*, and *stil* are normalized to that of
969 *α-tub*. Error bar indicates s.d. (*n*=3). (B) Representative images showing entire
970 ovarian morphology (left panels) and ovarioles immunostained with a germline
971 marker, Vasa (red), and nuclear staining with DAPI (blue) (right panels) from
972 *stil*-GLKD and the control with shRNA alone. Scale bar: 1 mm for whole ovaries
973 and 50 μm for ovarioles, respectively. (C) Quantification of the percentage of
974 germline cell-containing ovarioles in 2-3-days old females. Genotypes are
975 indicated below the graph and the number of germarium assessed is noted
976 above each bar. Error bars represent standard deviation (s.d.). (D)
977 Quantification of the percentage of developed ovarioles defined as ovarioles
978 that contain at least two egg chambers beyond the germarium. Genotypes are
979 indicated below the graph and the number of germarium assessed is noted
980 above each bar. Error bars represent standard deviation (s.d.). (E)
981 Representative images of TUNEL-positive apoptotic cells (green), Vasa (red),
982 and DAPI (blue) in control with shRNA alone and *stil*-GLKD germaria (white
983 dotted). Scale bar: 20 μm. (F) Quantification of apoptosis in germarium with
984 TUNEL assay in control and *stil*-GLKD. (G) Representative images of germaria
985 (white dotted) from $stil^{EY16156}$, $stil^{EY16156}$*; P35 OE* (*NGT40; NosGal4-VP16> P35*),
986 and $stil^{EY16156}$; *DIAP1 OE* (*NGT40; NosGal4-VP16> DIAP1*) immunostained

987 with Vasa (red) with DAPI (blue). Scale bar: 20 μm. (H) Quantification of the
988 percentage of germline cell-containing ovarioles in 2–3-day old females.
989 Genotypes are indicated below the graph and the number of germarium
990 assessed is noted above each bar. Error bars indicate standard deviation (s.d.).

991

992 **Figure 3. *stil* regulates *rpr* expression in female germline cells**

993 (A) Top 10 upregulated and downregulated genes in *stil*-deficient ovaries. Bars
994 indicate fold changes in *stil* mutant ovaries overexpressing (OE) of the
995 apoptosis inhibitor, P35 in germline cells (*stil*^{EY16156}*, NGT40; NosGal4-VP16>*
996 *P35*), compared to control with P35 OE in a heterozygous background
997 (*stil*^{EY16156}*/CyO, NGT40; NosGal4-VP16> P35*). Bars are according to adjusted
998 p-values (p-adj). (B) MA plot of apoptosis-related genes (GO:0006915) showing
999 their mean gene expression (CPM: counts per million) and fold change in
1000 *stil*^{EY16156}*; P35 OE* comparing *stil*^{EY16156}*/CyO; P35 OE*. Each dot represents an
1001 individual gene, with dot size inversely correlated with p-value adjusted (p-adj).
1002 Larger dots highlight genes with higher statistical significance. The red dots
1003 (upregulated genes) and blue dots (downregulated genes) represent the
1004 differentially expressed RNAs with fold threshold>2.0, and p-adj<0.01. (C) Top
1005 10 upregulated and downregulated genes related to apoptosis (GO:0006915).
1006 Bars represent fold changes and are colored by adjusted p-values (p-adj), as
1007 in (A). (D) Quantitative RT-PCR analysis of proapoptotic genes, *rpr* and *hid* in

1008 *stil*^{EY16156}*; P35 OE* and *stil*^{EY16156}*/CyO; P35 OE* ovaries. Expression levels were
1009 normalized to *αtub* with *rp49* as an internal control. Error bars indicate s.d. (*n*=3).
1010 (E) Immunofluorescence of Vasa (red) and DAPI (blue) in ovarioles from
1011 *stil*^{EY16156}*/CyO; rpr*^{87}/+, *stil*^{EY16156}*/CyO; rpr*^{87}*, stil*^{EY16156}*; rpr*^{87}/+, and *stil*^{EY16156}*;*
1012 *rpr*^{87}. Scale bar: 50 μm. (F) Quantification of the percentage of germline cell-
1013 containing ovarioles in 2-3-days old females. Genotypes of females and the
1014 number of germarium assessed are noted above each bar. Error bars represent
1015 standard deviation (s.d.). (G) Quantification of the percentage of developed
1016 ovarioles defined as ovarioles that contain at least two egg chambers beyond
1017 the germarium. Genotypes females and the number of germarium assessed
1018 are noted above each bar. Error bars represent standard deviation (s.d.). (H)
1019 Analysis of egg laying and hatching rate. Daily egg laying by three females
1020 indicated genotypes mated with three *y w* male and their hatching rate are
1021 shown (*n*=3). Error bar indicates s.d.

1022

1023 **Figure 4. Stil interacts with *rpr*-transcriptional control region to repress**
1024 **its expression**

1025 (A) Distribution of DamID peaks across entire genome categorized by genomic
1026 features including promoter (≤1, 1–2, and 2–3 kb), UTR, exon, intron, distal
1027 intergenic, and downstream. (B) The plot showing the $\log_2$ ratio of Dam-Stil
1028 peaks to Dam-alone control across the *rpr* genomic region. The blue bar on the

1029 bottom indicates the *rpr* gene body, and the arrow shows the direction of *rpr*
1030 transcription. Three independent biological replicates were performed for both
1031 Dam-Stil and Dam-alone and data were merged for visualization. (C) Schematic
1032 representation of the Stil full-length (Stil-FL), the truncated variants: Stil-NT (1st
1033 to 169th aa) and Stil-CT (169th to the end), and amino acid substitutions of the
1034 C2H2 zinc finger CCYC: Stil-AAYA. (D) *stil*^{EY16156} ovaries expressing Myc-
1035 tagged Stil variants corresponding to C in germline cells. Ovaries are
1036 immunostained with a germline marker, Vasa (red), and nuclear staining with
1037 DAPI (blue). Scale bar: 50 μm. (E) Quantification of the percentage of germline
1038 cell-containing ovarioles in 2-3 days-old females. Genotypes are indicated
1039 below the graph and the number of germarium assessed is noted above each
1040 bar. Error bars represent standard deviation (s.d.). (F) Quantification of the
1041 percentage of developed ovarioles defined as ovarioles that contain at least two
1042 egg chambers beyond the germarium. Genotypes are indicated below the
1043 graph and the number of germarium assessed is noted above each bar. Error
1044 bars indicate standard deviation (s.d.). (G) Schematic representation of *rpr*-
1045 GFP reporter containing the 5 kb upstream region of the *rpr* gene fused to GFP
1046 CDS. (H) Reporter assay in S2 cells followed by western blot analysis to detect
1047 GFP and α-Tubulin (αTub) as a loading control. Co-transfection of the *rpr*-GFP
1048 reporter and FLAG-tagged Stil variants were performed in S2 cells. The lower
1049 panel shows the signal ratio of GFP expression to αTub, normalized to that in
1050 cells transfected with the reporter alone. Error bars represent the standard

1051 deviation (s.d.) (n = 3).

1052

1053 **Figure 5. *stil* mutant germline stem cells resist apoptosis**

1054 (A) Fluorescent immunostaining with anti-Engrailed (red), anti-Vasa (green),
1055 and DAPI (blue) for terminal filaments of late 3rd instar larval (LL3) ovaries from
1056 the heterozygous control, *stil*^{EY16156}*/CyO* and *stil* mutant, *stil*^{EY16156}. Scale bar:
1057 50 μm. (B) Quantification of surviving germline cells in 3rd instar larval ovaries
1058 from *stil*^{EY16156}*/CyO* and *stil*^{EY16156}*.* (C) Immunostaining of Vasa (red) and DAPI
1059 (blue) in control, *Tkv.CA* (constitutive active Thickveins) *OE* (*NGT40; NosGal4-*
1060 *VP16>Tkv.CA*), and *bam* mutant (*bam*$^{\Delta 86}$) germaria (white dotted) in the control
1061 heterozygous (*stil*^{EY16156}*/CyO*) or *stil* mutant (*stil*^{EY16156}) background. Scale bar:
1062 20 μm. (D) Quantification germline cell-containing germaria per ovary in 2-3
1063 days-old females. Genotypes and the number of germarium assessed are
1064 indicated above each bar. Error bars represent standard deviation (s.d.). (E)
1065 Representative images of germaria (white dashed lines) showing TUNEL-
1066 positive apoptotic cells (green), Vasa (red), and DAPI (blue) in the control
1067 tumorous germaria (*stil*^{EY16156}*/CyO; Tkv.CA OE*) and tumorous germaria of *stil*
1068 mutant ovaries (*stil*^{EY16156}*; Tkv.CA OE*). White arrowheads indicate TUNEL-
1069 positive apoptotic cells. Scale bar: 20 μm. (F) Quantification of apoptosis in
1070 germaria from the control tumorous ovaries (*stil*^{EY16156}*/CyO; Tkv.CA OE*) and
1071 *stil* mutant ovaries (*stil*^{EY16156}*; Tkv.CA OE*). (G) MA plot of apoptosis-related

1072 genes showing the mean gene expression (CPM: counts per million) and fold
1073 change in *stil* mutant ovaries (*stil*^{EY16156}*; Tkv.CA OE*) compared to the control
1074 tumorous ovaries (*stil*^{EY16156}*/CyO; Tkv.CA OE*). Each dot represents an
1075 individual gene, with dot size inversely correlated with p-adj. The blue dots
1076 represent the downregulated genes with fold change<-2.0, and p-adj<0.01. (H)
1077 Quantitative RT-PCR analysis of *rpr* in the control tumorous ovaries
1078 (*stil*^{EY16156}*/CyO; Tkv.CA OE*) and *stil* mutant ovaries (*stil*^{EY16156}*; Tkv.CA OE*).
1079 Expression levels of an internal control, *rp49*, and *rpr* are normalized to that of
1080 *α-tub*. Error bars indicate s.d. (*n*=3).

1081

1082 **Figure 6. chromatin state changes in female germline cells during**
1083 **oogenesis**

1084 (A) ATAC-seq signal intensity (RPM-normalized) at the *rpr* locus in germline
1085 stem cells (GSCs: 2N and 4N) and nurse cells (NCs) at different ploidy levels
1086 (4C to 512C). The Y-axis is fixed at 0-30 PRM for all tracks. For 64C, 128C,
1087 256C, and 512C NCs, data from three biological replicates are averaged; all
1088 other samples are based on single replicates.
1089 (B) H3K9me3 ChIP-seq signal at the *rpr* locus in 4C GSCs and 4C NCs. (C)
1090 H3K27me3 ChIP-seq signal at the *rpr* locus in GSCs and stage 5 (st5) NCs.

1091

1092

1093 ## Supplementary Legends

1094 **Figure S1. *stil* function is indispensable in female germline cells not**

1095 **male germline cells**

1096 (A) Immunostaining of ovaries from *y w*, *stil*^{3}*/CyO*, *stil*^{3}*/Df*, and *stil*^{3}*/stil*^{EY16156}

1097 with antibody against Vasa (red) with DAPI (blue). Scale bar: 50 μm. (B)

1098 Quantification of the percentage of germline cell-containing ovarioles in 2-3

1099 days old females. (C) Immunostaining of the apical end of testes from

1100 *stil*^{EY16156}*/CyO* and *stil*^{EY16156} with anti-Vasa antibody (red) and DAPI (blue) (top

1101 panels). Seminal vesicles (SV) harboring sperms are also stained with DAPI

1102 (blue) (bottom panels). Asterisk denotes the apex of testis. Scale bar: 50μm

1103 (apical end of testes, top) and 20 μm (SV, bottom). (D) The numbers of egg

1104 laying and hatching rate. Daily egg laying by three *y w* females mated with three

1105 males of the indicated genotypes are shown (*n*=3). The number of ovarioles

1106 assessed is noted above each bar. Error bar indicates s.d.

1107

1108 **Figure S2. Germline knockdown of *stil*, but not somatic knockdown,**

1109 **specifically disrupts egg development**

1110 (A) Analysis of egg laying and hatching rates. The number of laid eggs and their

1111 hatching rates are measured daily for three females of the indicated genotypes:

1112 control, *stil*-germline knockdown (*stil*-GLKD) driven by *NGT40; NosGal4-VP16*,

1113 and *stil*-somatic knockdown (*stil*-STKD) driven by *tj-Gal4*, each mated with

1114 three *y w* males (*n* = 3). Error bars indicate standard deviation (s.d.). (B) RT-

1115 PCR analysis of *sxl* and the control, *α-tub* transcripts in ovaries and testes from
1116 control and *stil*-GLKD flies, respectively.

1117

1118 **Figure S3. Egg development is disrupted at the mid-stage of oogenesis**
1119 **in *stil* mutants rescued by P35 or DIAP**

1120 Immunostaining of ovarioles from *y w*, *stil*^{EY16156}/*CyO; P35 OE* (*NGT40;*
1121 *NosGal4-VP16> P35*), *stil*^{EY16156}*; P35 OE* and *stil*^{EY16156}*; DIAP OE* (*NGT40;*
1122 *NosGal4-VP16> DIAP1*) flies with antibody against Vasa (red) and DAPI (blue).
1123 The enlarged image highlights a degenerated egg chamber at the mid-stage of
1124 oogenesis in *stil*^{EY16156}*; P35 OE*. Scale bar: 50 μm.

1125

1126 **Figure S4. BED-type zinc finger of Stil and transcriptome analysis of**
1127 **germline-rescued *stil* mutant ovaries**

1128 (A) A schematic presentation of Stil protein, highlighting the BED-type zinc
1129 finger (BED, green) and the nuclear localization signal (NLS, blue). A multiple
1130 sequence alignment of Stil with three other proteins containing BED-type zinc
1131 finger motif is shown. The BED-type zinc finger motif consists of two cysteine
1132 and histidine residues (red) and aromatic residues (yellow) in the N-terminal
1133 region. (B) Transcriptome analysis of germline-rescued *stil* mutant ovaries
1134 expressing P35. Differential expressed genes (DEGs) are obtained with
1135 DEseq2. Volcano plot displays the adjusted *p*-value (*p*-adj) versus log2-fold

1136 change (log2FC) of expression level in *stil*^{EY16156}*; P35 OE* compared to that in
1137 *stil*^{EY16156}*/CyO; P35 OE*. Significantly upregulated genes (log2FC > 1, *p*-adj <
1138 0.01) and downregulated genes (log2FC < -1, *p*-adj < 0.01) are highlighted in
1139 red and blue, respectively, while non-DEGs are shown in black.

1140

1141 **Figure S5. *rpr*, but not *hid*, plays a central role in *stil*-deficient female**
1142 **germline cell death**

1143 (A-C) Quantitative RT-PCR are performed on ovaries from germline-rescued
1144 *stil* mutants, as well as ovaries and testes with germline-specific *stil* knockdown
1145 using distinct drivers. Expression levels are normalized to *αtub* with *rp49*
1146 serving as an internal control. (A) Early-stage ovaries are isolated by dissecting
1147 stage 4–5 oocytes from *stil*^{EY16156}*/CyO; P35 OE* and *stil*^{EY16156}*; P35 OE* flies (B)
1148 *stil* knockdown in female germline cells is achieved using *NGT40-Gal4;*
1149 *NosGal4-VP16*, *Bam-Gal4*, and *matα-tub-Gal4* drivers. (C) *stil* knockdown in
1150 male germline cells is achieved using *NGT40-Gal4; NosGal4-VP16* and *Bam-*
1151 *Gal4* drivers. Error bars represent standard deviation (s.d.). (D) Immunostaining
1152 of *stil*^{EY16156}*; hid*^{05014}*/+* and *stil*^{EY16156}*; hid*^{05014}*/Df(3L)X14* ovaries with antibody
1153 against Vasa (red) with DAPI (blue). Scale bar: 50 μm. (E) Quantification of the
1154 percentage of germline cell-containing ovarioles in 2-3-days old females. The
1155 number of ovarioles assessed is noted above each bar.

1156

1157 **Figure S6. Stil variants localization and control validation in S2 reporter**

1158 **assay**

1159 (A) Immunofluorescence images showing Myc-tagged Stil variants (green) and

1160 DNA (DAPI, blue) in stage 3~4 egg chambers of the ovaries. Insets show

1161 enlarged views of nurse cell nuclei. Scale bar: 50 μm (egg chamber) and 20 μm

1162 (nurse cell nuclei). (B) Immunostaining of S2 cells expressing FLAG-tagged Stil

1163 variants with an anti-FLAG (green) antibody and DAPI (blue). (C) Schematic

1164 representation of the *tubP*-GFP reporter construct, in which the 2.4-kb

1165 upstream region of the *αTub84B* gene is fused to GFP. (D) Reporter assay in

1166 S2 cells followed by western blot analysis to detect GFP expression.

1167 Arrowheads indicate Stil-variant proteins. *α*-Tubulin (αTub) is used as a loading

1168 control. The lower panel quantifies the GFP/αTub signal ratio, normalized to

1169 that in S2 cells transfected with the reporter alone. Error bars indicate standard

1170 deviation (s.d.) (n = 3).

1171

1172

Figure 1

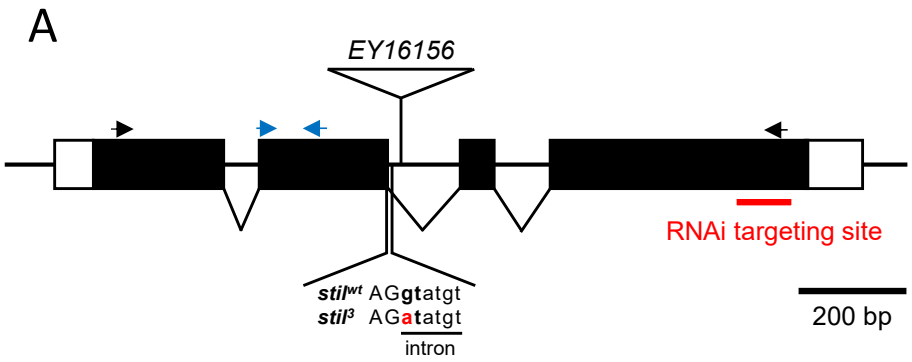
A
EY16156
RNAi targeting site
stil^wt AGgtatgt
stil^3 AGatatgt
intron
200 bp

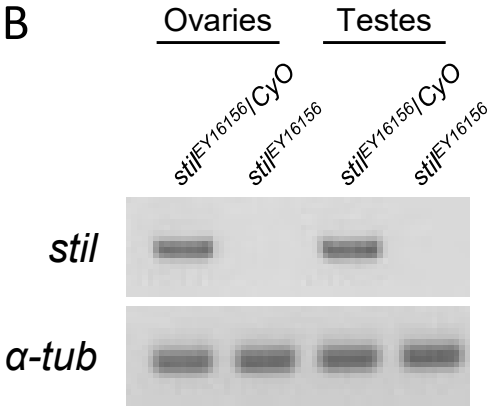
B
Ovaries
Testes
stil^EY16156/CyO
stil^EY16156
stil^EY16156/CyO
stil^EY16156
stil
α-tub

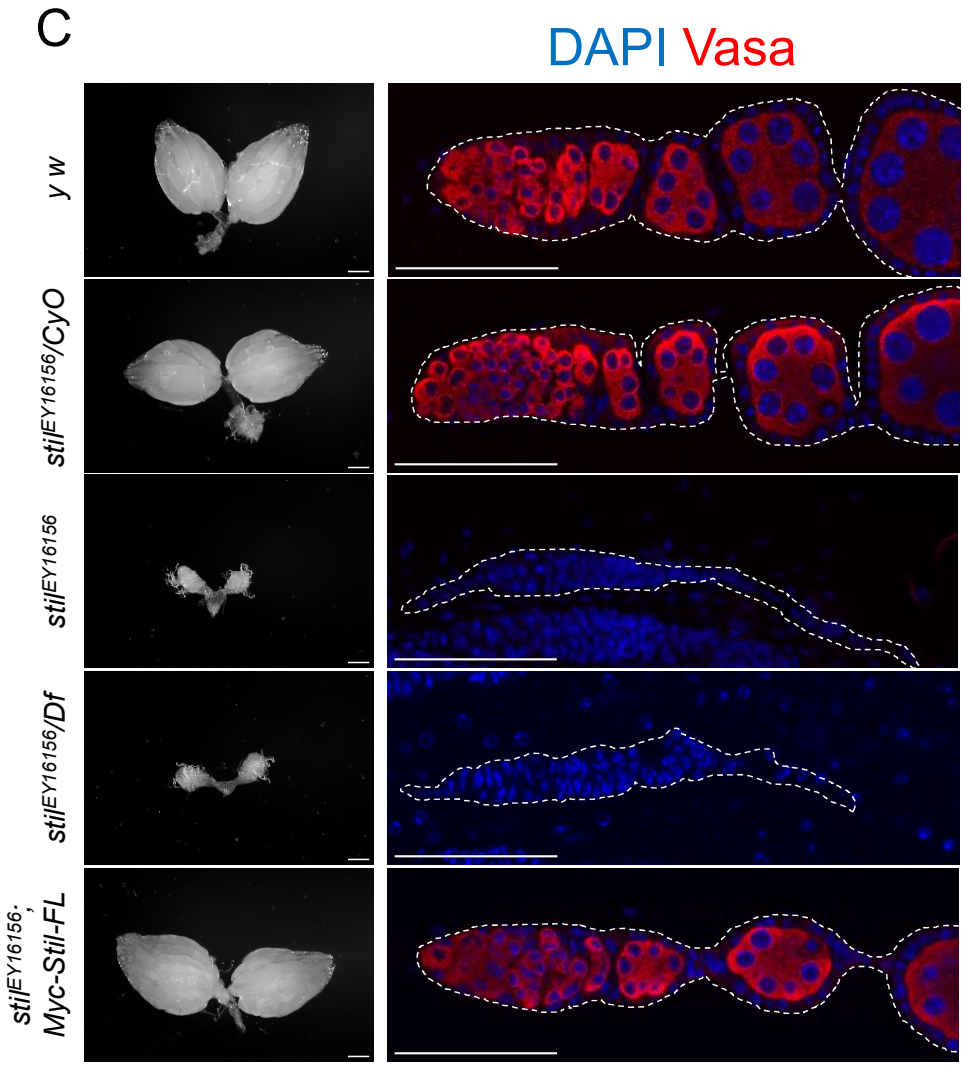
C
DAPI Vasa
y w
stil^EY16156/CyO
stil^EY16156
stil^EY16156/Df
stil^EY16156; Myc-Stil-FL

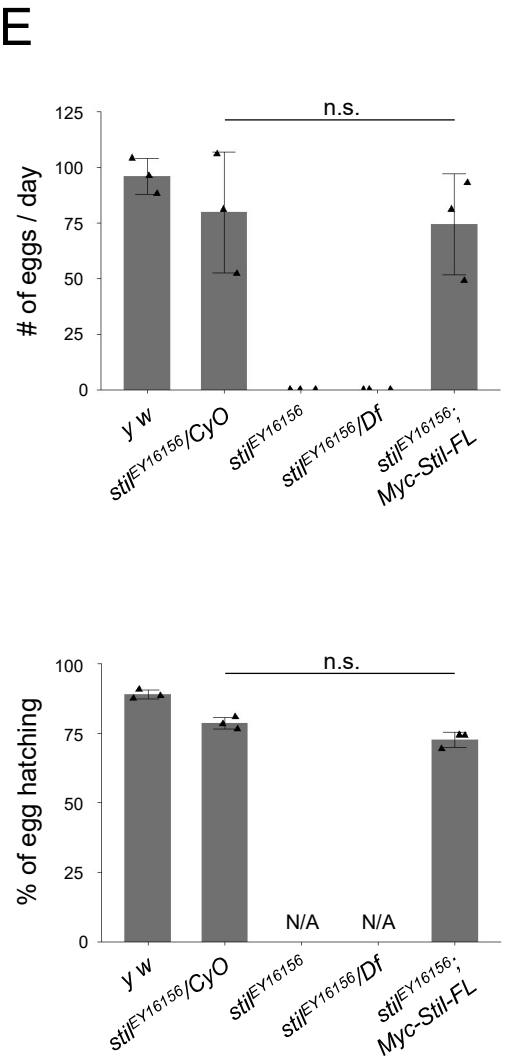
E
n.s.
# of eggs / day
125
100
75
50
25
0
y w
stil^EY16156/CyO
stil^EY16156
stil^EY16156/Df
stil^EY16156; Myc-Stil-FL
n.s.
% of egg hatching
100
75
50
25
0
N/A
N/A

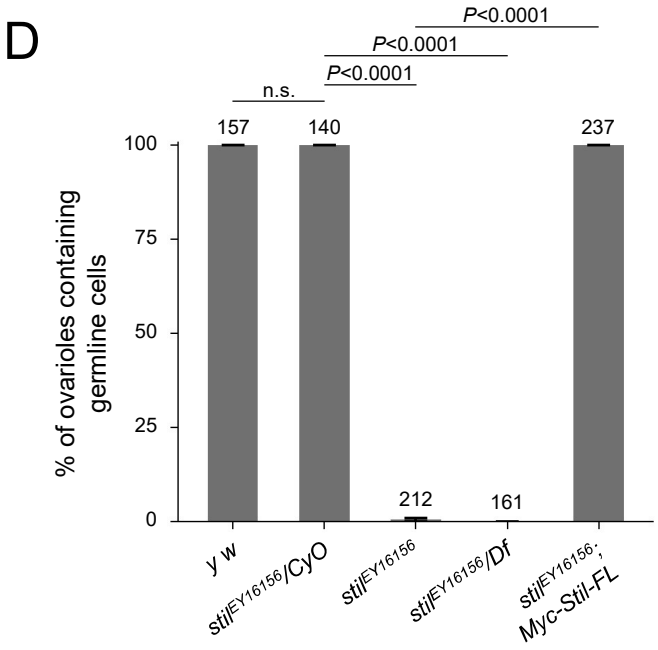
D
P<0.0001
P<0.0001
P<0.0001
n.s.
% of ovarioles containing germline cells
100
75
50
25
0
157
140
212
161
237
y w
stil^EY16156/CyO
stil^EY16156
stil^EY16156/Df
stil^EY16156; Myc-Stil-FL

Figure 2

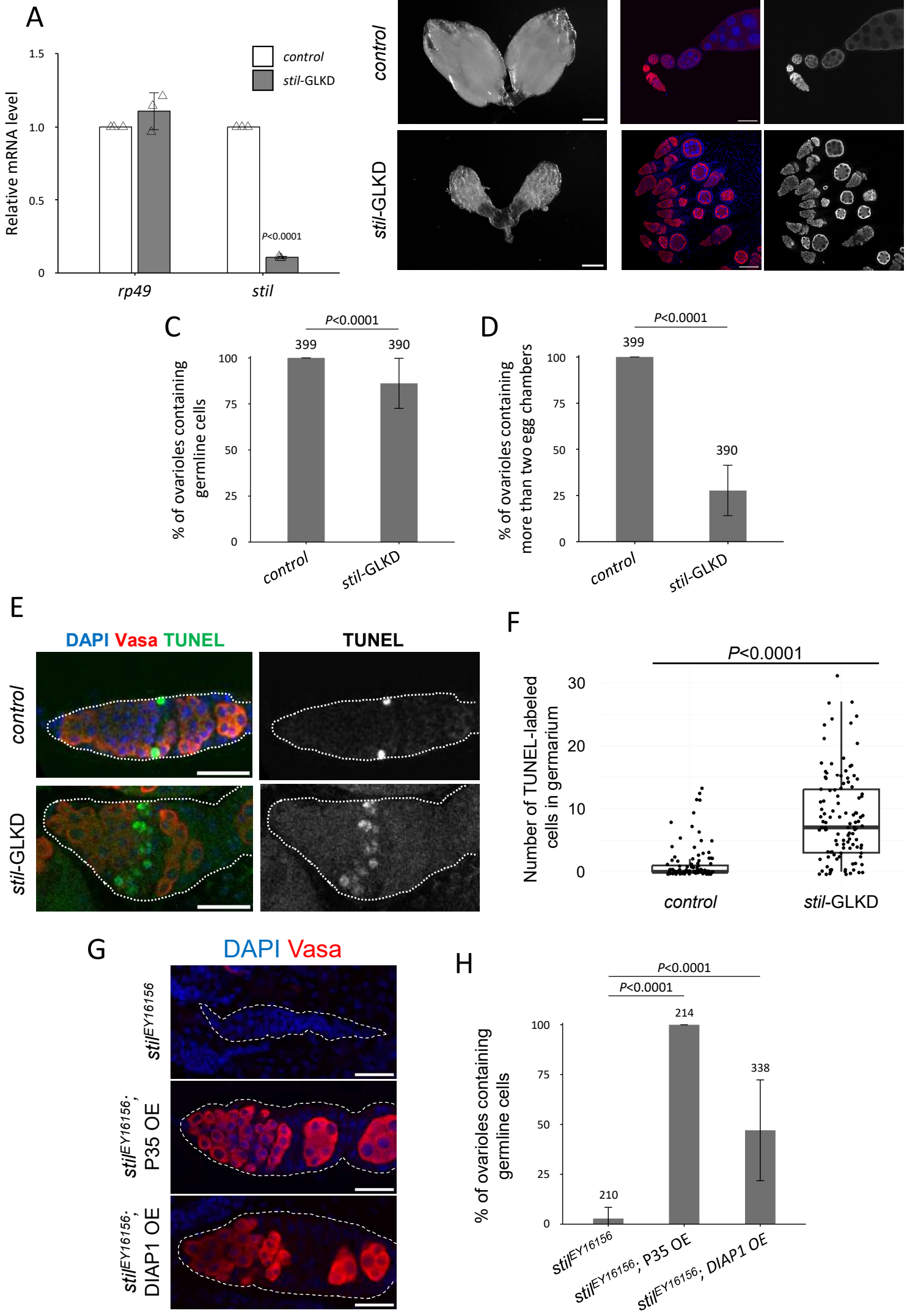
A
Relative mRNA level
1.5
1.0
0.5
0
control
stil-GLKD
P<0.0001
rp49
stil
B
DAPI Vasa
Vasa
control
stil-GLKD
C
P<0.0001
399
390
% of ovarioles containing germline cells
100
75
50
25
0
control
stil-GLKD
D
P<0.0001
399
390
% of ovarioles containing more than two egg chambers
100
75
50
25
0
control
stil-GLKD
E
DAPI Vasa TUNEL
TUNEL
control
stil-GLKD
F
P<0.0001
Number of TUNEL-labeled cells in germarium
30
20
10
0
control
stil-GLKD
G
DAPI Vasa
stilEY16156
stilEY16156; P35 OE
stilEY16156; DIAP1 OE
H
P<0.0001
P<0.0001
214
338
210
% of ovarioles containing germline cells
100
75
50
25
0
stilEY16156
stilEY16156; P35 OE
stilEY16156; DIAP1 OE

Figure 3

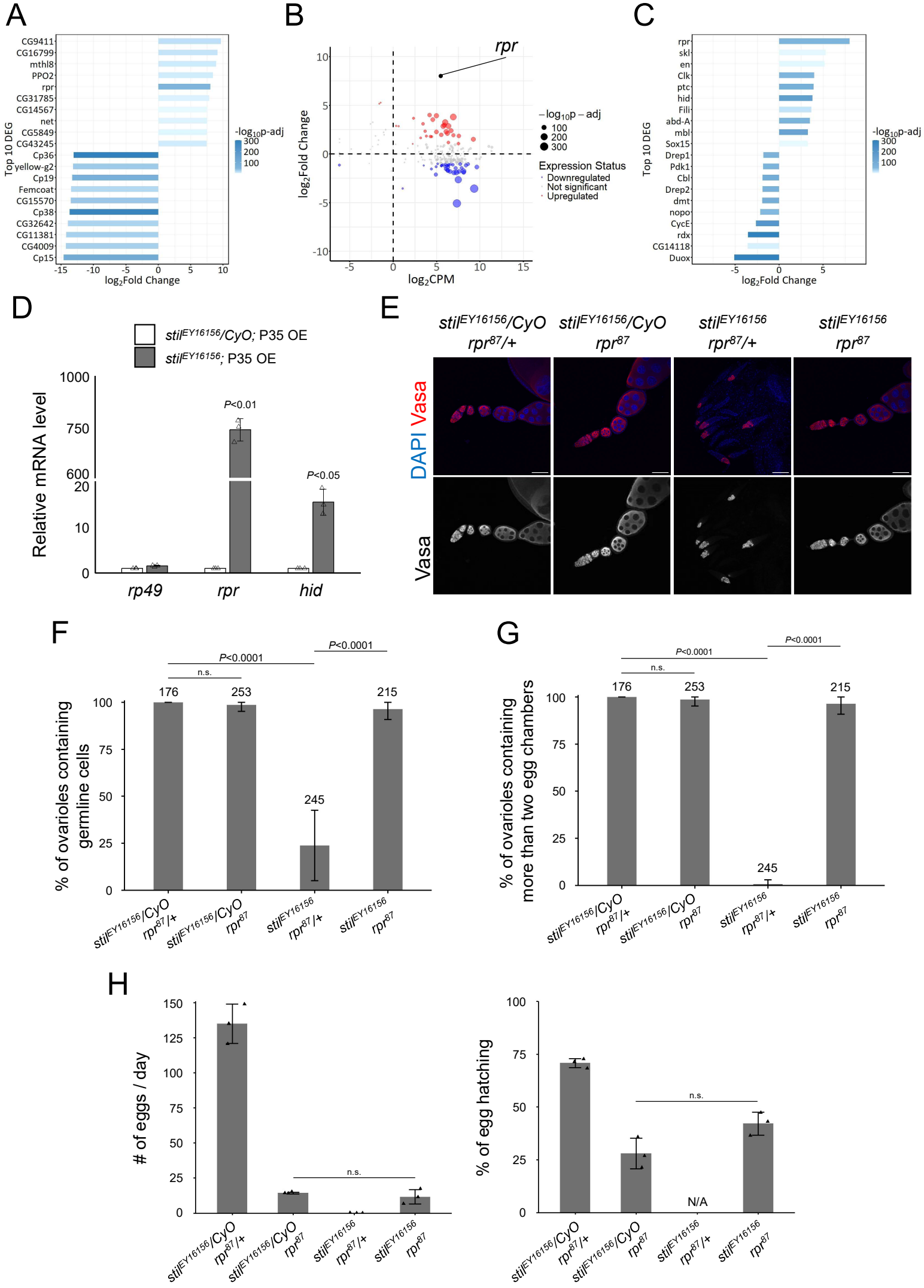
A
CG9411
CG16799
mthl8
PPO2
rpr
CG31785
CG14567
net
CG5849
CG43245
Cp36
yellow-g2
Cp19
Femcoat
CG15570
Cp38
CG32642
CG11381
CG4009
Cp15
Top 10 DEG
log2Fold Change
-log10p-adj
300
200
100
B
rpr
log2Fold Change
log2CPM
−log10p − adj
100
200
300
Expression Status
Downregulated
Not significant
Upregulated
C
rpr
skl
en
Clk
ptc
hid
Fili
abd-A
mbl
Sox15
Drep1
Pdk1
Cbl
Drep2
dmt
nopo
CycE
rdx
CG14118
Duox
Top 10 DEG
log2Fold Change
-log10p-adj
300
200
100
D
stilEY16156/CyO; P35 OE
stilEY16156; P35 OE
Relative mRNA level
P<0.01
P<0.05
rp49
rpr
hid
E
stilEY16156/CyO rpr87/+
stilEY16156/CyO rpr87
stilEY16156 rpr87/+
stilEY16156 rpr87
DAPI Vasa
Vasa
F
P<0.0001
P<0.0001
n.s.
% of ovarioles containing germline cells
176
253
245
215
stilEY16156/CyO rpr87/+
stilEY16156/CyO rpr87
stilEY16156 rpr87/+
stilEY16156 rpr87
G
P<0.0001
P<0.0001
n.s.
% of ovarioles containing more than two egg chambers
176
253
245
215
stilEY16156/CyO rpr87/+
stilEY16156/CyO rpr87
stilEY16156 rpr87/+
stilEY16156 rpr87
H
# of eggs / day
n.s.
stilEY16156/CyO rpr87/+
stilEY16156/CyO rpr87
stilEY16156 rpr87/+
stilEY16156 rpr87
% of egg hatching
n.s.
N/A
stilEY16156/CyO rpr87/+
stilEY16156/CyO rpr87
stilEY16156 rpr87/+
stilEY16156 rpr87

Figure 4

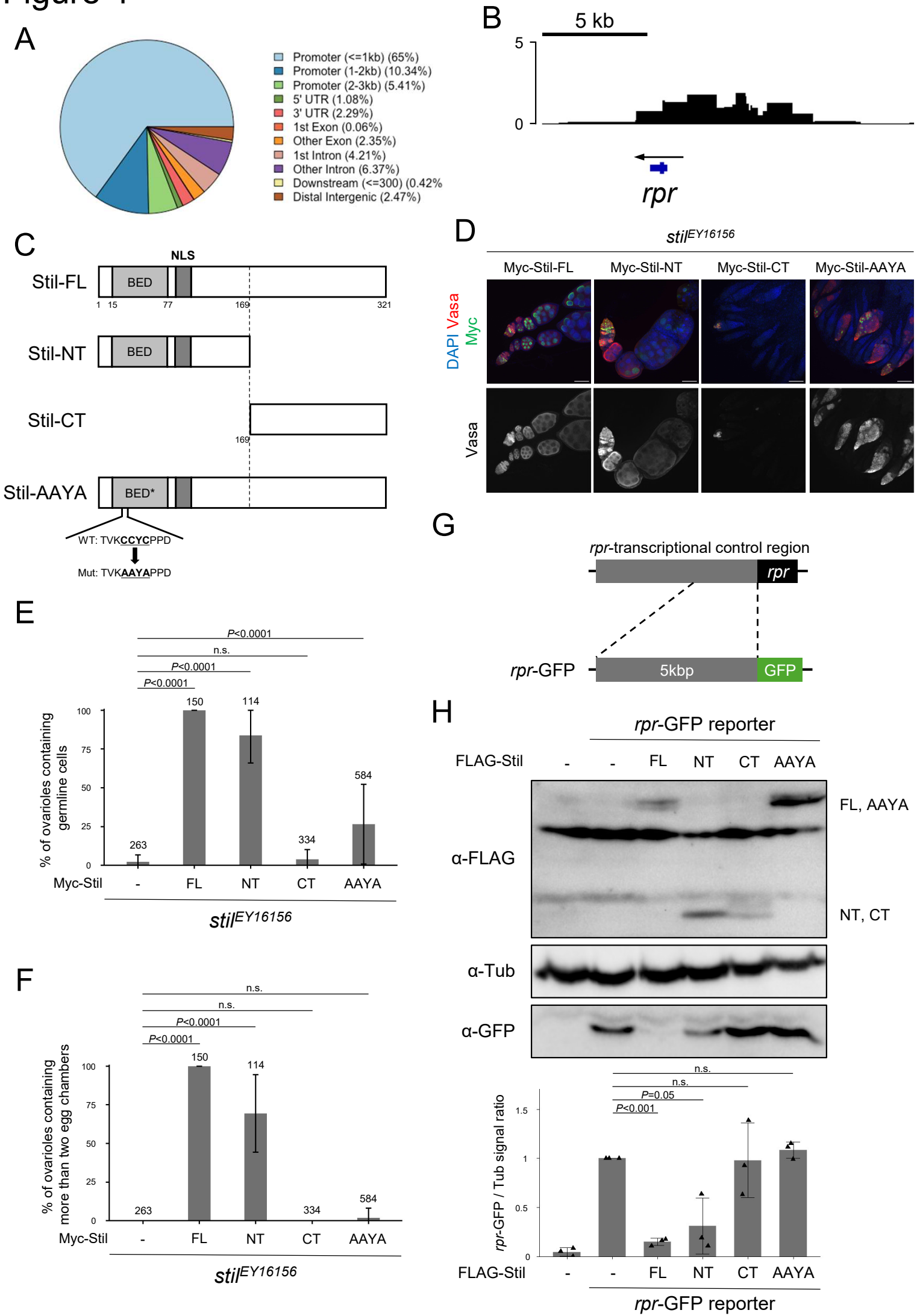
A
Promoter (<=1kb) (65%)
Promoter (1-2kb) (10.34%)
Promoter (2-3kb) (5.41%)
5' UTR (1.08%)
3' UTR (2.29%)
1st Exon (0.06%)
Other Exon (2.35%)
1st Intron (4.21%)
Other Intron (6.37%)
Downstream (<=300) (0.42%
Distal Intergenic (2.47%)
B
5 kb
5
0
rpr
C
NLS
Stil-FL
BED
1 15 77 169 321
Stil-NT
BED
Stil-CT
169
Stil-AAYA
BED*
WT: TVKCCYCPPD
Mut: TVKAAYAPPD
D
stilEY16156
Myc-Stil-FL
Myc-Stil-NT
Myc-Stil-CT
Myc-Stil-AAYA
DAPI Vasa Myc
Vasa
G
rpr-transcriptional control region
rpr
rpr-GFP
5kbp
GFP
E
P<0.0001
n.s.
P<0.0001
P<0.0001
% of ovarioles containing germline cells
100
75
50
25
0
263
150
114
334
584
Myc-Stil
-
FL
NT
CT
AAYA
stilEY16156
F
n.s.
n.s.
P<0.0001
P<0.0001
% of ovarioles containing more than two egg chambers
100
75
50
25
0
263
150
114
334
584
Myc-Stil
-
FL
NT
CT
AAYA
stilEY16156
H
rpr-GFP reporter
FLAG-Stil
-
-
FL
NT
CT
AAYA
α-FLAG
FL, AAYA
NT, CT
α-Tub
α-GFP
n.s.
n.s.
P=0.05
P<0.001
rpr-GFP / Tub signal ratio
1.5
1
0.5
0
FLAG-Stil
-
-
FL
NT
CT
AAYA
rpr-GFP reporter

Figure 5

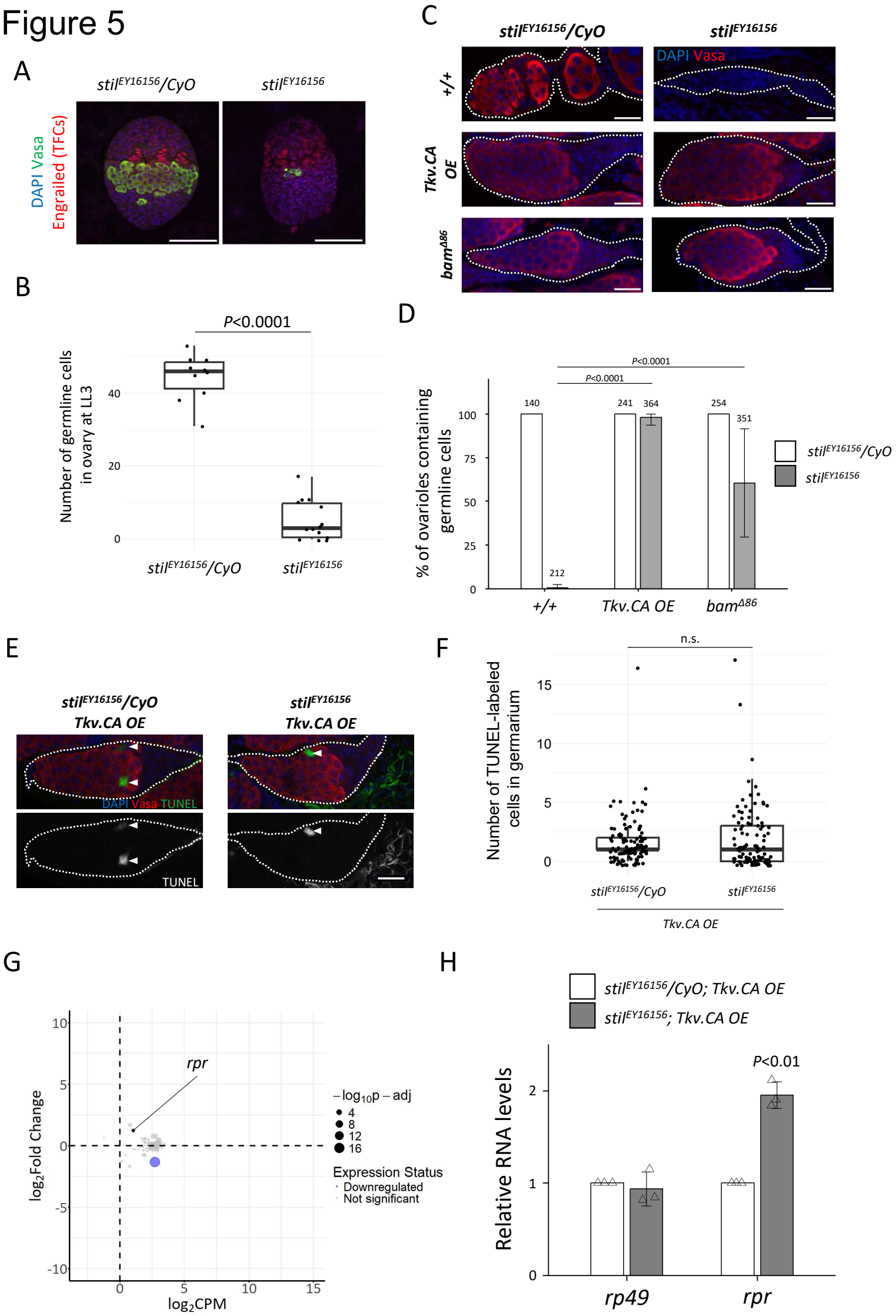
A
stilEY16156/CyO
stilEY16156
DAPI Vasa
Engrailed (TFCs)
B
P<0.0001
Number of germline cells in ovary at LL3
40
20
0
stilEY16156/CyO
stilEY16156
C
stilEY16156/CyO
stilEY16156
+/+
Tkv.CA OE
bamΔ86
DAPI Vasa
D
P<0.0001
P<0.0001
% of ovarioles containing germline cells
100
75
50
25
0
140
212
241
364
254
351
+/+
Tkv.CA OE
bamΔ86
stilEY16156/CyO
stilEY16156
E
stilEY16156/CyO Tkv.CA OE
stilEY16156 Tkv.CA OE
DAPI Vasa TUNEL
TUNEL
F
n.s.
Number of TUNEL-labeled cells in germarium
15
10
5
0
stilEY16156/CyO
stilEY16156
Tkv.CA OE
G
rpr
log2Fold Change
10
5
0
-5
-10
0
5
10
15
log2CPM
−log10p−adj
4
8
12
16
Expression Status
Downregulated
Not significant
H
stilEY16156/CyO; Tkv.CA OE
stilEY16156; Tkv.CA OE
P<0.01
Relative RNA levels
2
1
0
rp49
rpr

Figure 6

A

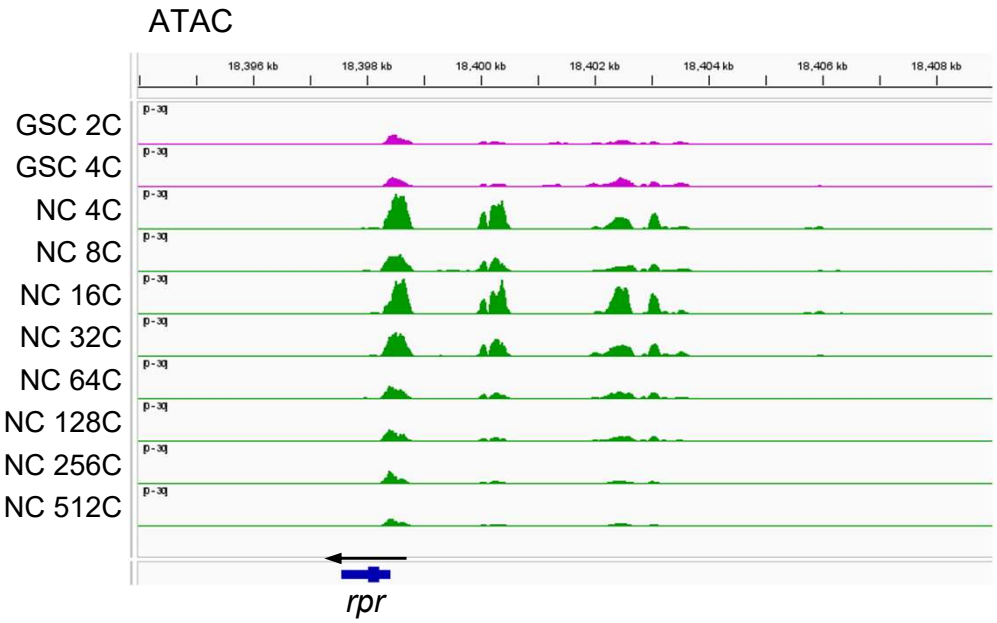
ATAC
18,396 kb
18,398 kb
18,400 kb
18,402 kb
18,404 kb
18,406 kb
18,408 kb
GSC 2C
GSC 4C
NC 4C
NC 8C
NC 16C
NC 32C
NC 64C
NC 128C
NC 256C
NC 512C
rpr

B

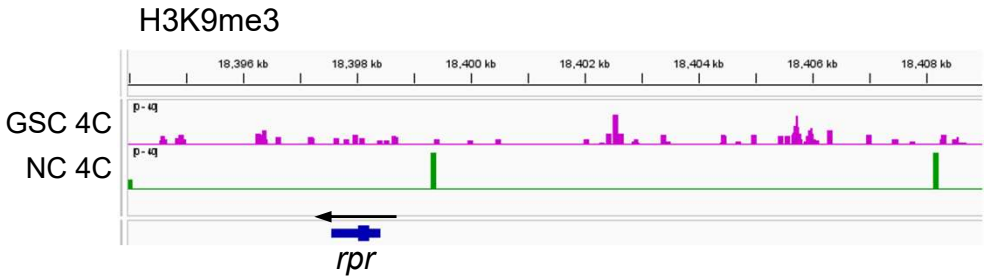
H3K9me3
18,396 kb
18,398 kb
18,400 kb
18,402 kb
18,404 kb
18,406 kb
18,408 kb
GSC 4C
NC 4C
rpr

C

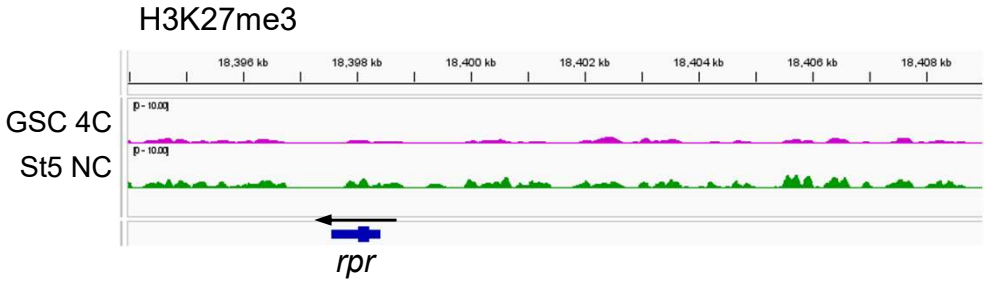
H3K27me3
18,396 kb
18,398 kb
18,400 kb
18,402 kb
18,404 kb
18,406 kb
18,408 kb
GSC 4C
St5 NC
rpr